KTH Electrical Engineering

On Design of a Compact Primary Switched Conversion System for Electric Railway Propulsion

Tommy Kjellqvist

Royal Institute of Technology
School of Electrical Engineering
Electrical Machines and Power Electronics
Stockholm 2009

Submitted to the School of Electrical Engineering, KTH, in partial fulfilment of the requirements for the degree of Doctor of Philosophy.

Copyright © Tommy Kjellqvist, Sweden, 2009
Printed in Sweden
Universitetsservice US-AB

TRITA–EE 2009:029
ISSN 1653–5146
ISBN 978–91–7415–327–9

This document was prepared using LaTeX.

Abstract

In this thesis, a compact and light primary switched conversion system for AC-fed railway propulsion is investigated. It is characterized by soft switching of all converter stages and a source commutated primary converter comprising series connected valves. Both weight and volume of the conversion system are reduced significantly compared to a conventional system with a low frequency transformer.

The conversion system is made up of N isolated AC/DC conversion cells, each comprising a cycloconverter and a voltage source converter (VSC) coupled by a medium frequency transformer. The cells are series connected on the AC side and connected to a common DC-link. Thus, $2N + 1$ voltage levels can be synthesized at the AC terminal and the voltage stress on the transformer and line filter is reduced compared to a one cell solution. Series connection of semiconductor valves allows independent choice of blocking voltage and number of converter cells. Choosing two converter cells is an attractive compromise. Five level output reduces the harmonic distortion and simplify transformer and line filter design while keeping the complexity of the conversion system low.

The mutually commutated converter (MCC) allows a transformer frequency in the range of 4 to 8 kHz without derating the line side converter due to zero voltage switching of the VSC. Modern magnetic materials, like high silicon steel, amorphous and noncrystalline materials allow design of the transformer with high efficiency at elevated frequencies.

In a 15 kV system, the peak voltage at the catenary is typically beyond 32 kV which is far beyond the voltage capability of currently available semiconductors. Therefore, several semiconductors are connected in series. Favourable commutation conditions and a new gate drive arrangement allow snubberless commutation of the primary converter stage. Thus, the primary converter can be highly integrated, reducing both weight and volume. The conversion system can be placed on the roof or in the underframe without compromising efficiency or vehicle performance.

The feasibility of the conversion concept has been demonstrated by means of a down-scaled prototype. Snubberless commutation of series connected valves is demonstrated.

Keywords: *Isolated AC/DC Converter, Mutual Commutation, Soft Switching, Cycloconverter, Medium-Frequency Transformer, Electric Railway Propulsion*

Acknowledgments

This research project was funded by the Swedish Railway Administration, which is gratefully acknowledged.

First of all, I would like to thank my supervisor Stefan Östlund for support throughout the project. In the same context I would like to thank Staffan Norrga who offered guidance during the work.

I would like to thank the members of the steering committee: Stefan Östlund, Staffan Norrga, Hans-Peter Nee, Edvard Friman, and Per Bengtsson. They have all contributed with information and valuable feedback.

Several people have helped out in the development of the laboratory prototype. Jan-Ove Brännvall helped out by manufacturing mechanical parts. Jan Timmerman and later Stefan Meier also helped out in the laboratory. Sven Hedin has helped in the manufacturing of the many valves in the prototype converter. You have all been invaluable while working in the lab.

I want to express my appreciation to current and former companions at the coffee table. In this context I thank my brother Peter Kjellqvist for introducing me at the Division of Electrical Machines and Power Electronics.

Last but not least I wish to thank my cohabitee Jenny Hylin for her support and my son Anton for his cheerful mood.

Stockholm, May 2009
Tommy Kjellqvist

Contents

1 Introduction **1**

1.1 Background 1
1.2 Objectives 3
1.3 Scientific Contributions 3
1.4 Outline of the Thesis 4
1.5 List of Publications 4

2 Survey of Related Topologies **7**

2.1 Conventional Drive System 7
2.2 Direct Conversion 8
2.3 Cascaded H-bridges 11
2.4 Modular Multilevel Converter 12
2.5 Transformerless Topology 15

3 Medium Frequency Conversion System **17**

3.1 Topology 17
3.2 Voltage Source Converter 19
3.3 Medium Frequency Transformer 20
3.3.1 Transformer Fundamentals 20
3.3.2 Core Material 21
3.3.3 The Transformer Geometry 25
3.3.4 Optimization of the Transformer 27
3.4 Cycloconverter 30
3.4.1 Switching Device 31
3.4.2 Snubber Circuit 33
3.4.3 Energy Recovery 35
3.4.4 Signalling 39
3.4.5 Reliability and Lifetime 41
3.4.6 Redundancy 42

3.5 Filtering 45
3.6 Drive Cycle Simulation 47

4 Prototype **51**
4.1 Main Circuit 51
4.2 Modulation and Control 52
4.3 Cycloconverter 54
4.3.1 Signalling 58
4.3.2 Cooling 59
4.3.3 Interconnect 59
4.3.4 Power Supply 60
4.3.5 Gate Drive and Snubber Circuit 60
4.3.6 Logic 60
4.4 Transformer 60
4.5 VSC 62
4.6 Experimental Results 62

5 Conclusions and Future Work **67**
5.1 Conclusions 67
5.2 Future Work 69

References **71**

Publication I **77**

Publication II **89**

Publication III **99**

Publication IV **109**

Publication V **119**

1 Introduction

1.1 Background

Railway electrification started in the beginning of the 20th century. The propulsion system at that time consisted of a universal motor fed by a step-down transformer and speed control was achieved by varying the motor voltage by means of a mechanical tap-changer. The frequency had to be limited due to the inductance of the machine and $16\,^2/_3\,\mathrm{Hz}$ is common in countries where the railway was electrified early (Germany, Austria, Switzerland, Norway and Sweden). Countries where the railway was electrified later use industrial frequency.

The low frequency strongly influences the design of the electrical equipment, especially the size of the on-board traction transformer. The weight of the transformer constitutes a significant part of the vehicle weight and has a significant impact on the vehicle design. The transformer is generally heavily loaded in order to reduce its weight, which leads to poor efficiency and large auxiliary systems for cooling. The weight of a conventional traction transformer is in the range of $2-4\,\mathrm{kg/kVA}$. The weight of the transformer is not necessarily a drawback in a locomotive where high weight is necessary in order to provide tractive effort without slipping. However, for fast passenger trains the trend is towards so called Electric Multiple Units (EMUs). Instead of having a dedicated locomotive, the propulsion system is distributed throughout the train and the demand for low weight is stronger.

There is a trend towards multiple propulsion systems for both locomotives and EMUs. On a deregulated market, trains operate across country borders from multiple voltage levels. Therefore, there is a need for traction

systems that can operate from multiple electric sources like 15 kV 16 2/3 Hz, 25 kV 50 Hz, 3000 V DC, or 1500 V DC. The weight of the transformer increases further as it has to be adapted to multiple frequencies and voltages. Dual system locomotives operate with electrical power on electrified lines and operated with power from a diesel engine on non-electrified lines. Thus, multiple propulsion systems add to the vehicles weight and share limited space onboard the vehicle.

The traction transformer is normally located in the underframe or on the roof. Accessibility constraints on modern rail vehicles call for low floor across the whole car body which limits the space available to traction equipment. The volume of the equipment placed on the roof is not necessarily constrained. However, placing the transformer on the roof significantly elevate the center of gravity which has a negative impact on the vehicle performance.

Systems to increase the transformer frequency have been studied in the past [1–11]. A primary conversion stage has to be added on the primary side of the transformer. This represents a technological difficulty as the catenary voltage is far beyond the blocking voltage of available switching devices. The primary converter is a new component in the system and its high component count is associated with lower reliability. Also, it adds weight to the conversion system and the weight savings on the transformer can be eradicated by the weight of the primary converter. Therefore, the frequency must by high enough to provide a substantial weight saving on the transformer and the complexity of the primary converter must be low.

The Medium Frequency Transformer (MFT) concept is currently most suitable in EMU applications where the drawback of the size and weight of the transformer is most pronounced. Therefore, this thesis is focused mainly on a converter system with a rating in the range of 1 MVA. In a later stage the advantages of the MFT concept, like high efficiency, may overweight the disadvantages even in locomotives.

1.2 Objectives

Even though MFT based solutions was first investigated in the seventies [1], none of the solutions have reached the market. Weight reduction of 50% and minimal volume reduction has been reported [7, 10, 11]. In the author's opinion, some of the main reasons for the previously proposed MFT concepts not yet being commercially successful are as follows.

- The complexity of the conversion system is high. The insulation has to be coordinated between a high number of converter stages.
- The transformer weight and volume is high. The transformer frequency is not high enough to compensate for the increased complexity of the transformer.

The MFT based solutions are studied in general and the Mutually Commutated Converter (MCC) system is studied in detail.

The objectives of the work are summarized below.

- Identify a suitable conversion system topology.
- Establish an appropriate transformer frequency.
- Propose a suitable transformer design.
- Demonstrate the feasibility of the selected topology by means of a prototype.

1.3 Scientific Contributions

The list below summarizes the main contributions presented in this thesis.

- A transformer topology suitable for conversion systems in the lower power range (1 MVA) is presented. The electrical and thermal be-

haviour is investigated analytically in [Publication I] and verified experimentally in [Publication V].

- A new gate drive that, in combination with source commutation of the primary converter, allows snubberless commutation of series connected IGBTs is presented in [Publication IV]. Snubberless commutation is possible which simplifies integration and improve efficiency.

- The feasibility of the MCC topology in railway traction is demonstrated by means of a prototype.

1.4 Outline of the Thesis

Chapter 2 gives a survey of topologies suitable for line side conversion systems.

Chapter 3 gives an overview of the studied medium frequency conversion system.

Chapter 4 gives on overview of the prototype development and some experimental results.

Chapter 5 summarizes the work and gives directions for future research.

1.5 List of Publications

This doctoral thesis includes the following publications:

Publication I deals with the design of a medium frequency transformer for EMU applications. An electro-thermal model coupled to the geometry of the transformer is developed. The model is used for preliminary optimization of the transformer geometry.

T. Kjellqvist, S. Norrga, and S. Östlund, "Design considerations for a medium frequency transformer in a line side power conversion system," *IEEE 35th Annual Power Electronics Specialists Conference, PESC '04*, Aachen, Germany, 2004.

Publication II deals with switching losses in the snubbered Voltage Source Converter (VSC). Switching losses in hard- and soft switching are measured and the result is used to derive a suitable transformer frequency.

T. Kjellqvist, S. Norrga, and S. Östlund, "Switching Frequency Limit for Soft-Switching MF Transformer System for AC-fed Traction," *IEEE 36th Power Electronics Specialists Conference,PESC '05*, Recife, Brazil, 2005.

Publication III deals with the harmonic content of the MCC. The low frequency harmonics, inherent to the MCC, are studied and its impact on the psophometric current is derived.

T. Kjellqvist and S. Norrga, "Harmonic Mitigation in Single Phase Mutually Commutated Converter Systems," *IEEE 37th Power Electronics Specialists Conference, PESC '06*, Jeju, Korea, 2006.

Publication IV describes a method to control the switching trajectories of the Insulated Gate Bipolar Transistor (IGBT) in a source commutated converter. The turn-on voltage waveform is controlled without increased delay time. The IGBT is used in its linear region in order to clamp the voltage across the anti-parallel diode.

T. Kjellqvist, S. Östlund, and S. Norrga, "Active Snubber Circuit for Source Commutated Converters Utilizing the IGBT in the Linear Region," *IEEE Transactions on Power Electronics*, vol. 23, 2008, pp. 2595-2601.

Publication V presents a transient thermal model of the medium frequency transformer. The model is verified by measurements on the prototype transformer.

Kjellqvist, T.; Norrga, S.; Östlund, S; Ilves, K., "Thermal Evaluation of a Medium Frequency Transformer in a Line Side Conversion System", Accepted for publication in the Proceedings of the *13th International European Power Electronics Conference and Exhibition, EPE '09*, Barcelona, Spain, Sept. 2009

In addition, during the course of work, the author has either authored or co-authored the following publications:

- P. Kjaer, T. Kjellqvist, and C. Delaloye, "Estimation of field current in vector-controlled synchronous machine variable-speed drives employing brushless asynchronous exciters," *IEEE Transactions on Industry Applications*, vol. 41, 2005, pp. 834-840.

- T. Kjellqvist and S. Norrga, "Active snubber circuit for source commutated converters utilizing the IGBT in the linear region," *European Conference on Power Electronics and Applications, EPE '07*, Aalborg, Denmark, 2007.

- Meier, S.; Kjellqvist, T.; Norrga, S.; Nee, H.-P., "Design Considerations for Medium-Frequency Power Transformers in Offshore Wind Farms", Accepted for publication in the Proceedings of the *13th International European Power Electronics Conference and Exhibition, EPE '09*, Barcelona, Spain, Sept. 2009.

2 Survey of Related Topologies

This chapter gives an introduction to medium frequency transformer topologies as well as state of the art in electric railway traction.

2.1 Conventional Drive System

A state of the art drive system is depicted in Figure 2.1. The Line Converter Module (LCM), Motor Converter Module (MCM) and Auxiliary Converter Module (ACM) are all interconnected by a stiff DC-link. The dominating traction motor is the induction machine due to its robustness and the possibility to feed multiple machines from a single inverter. The topology is highly modular in that the LCM and MCM are identical. The VSC based active rectifier offers bidirectional power flow, unity power factor as well as low harmonic distortion.

The low voltage side of the transformer is usually divided into two or more separate windings. This way some redundancy is provided. The converters

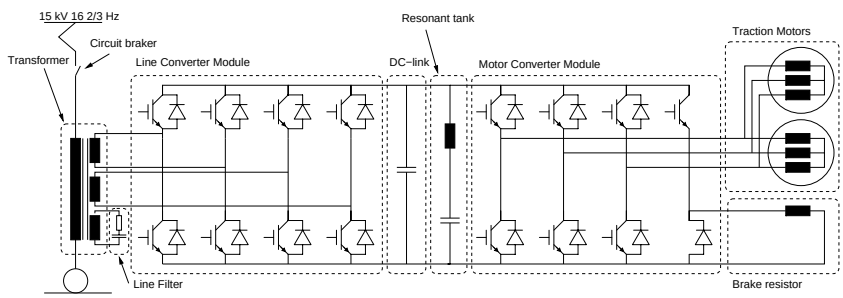

Figure 2.1: State of the art drive system for AC-fed propulsion.

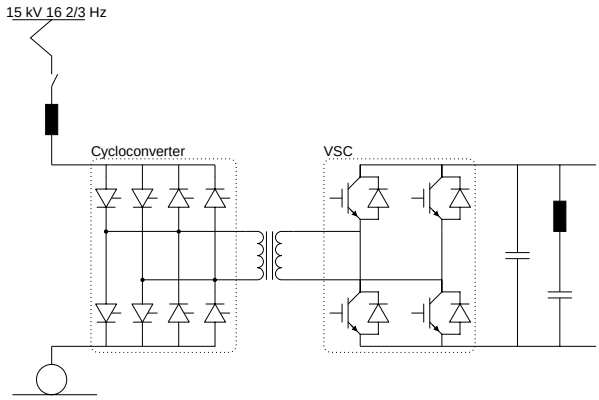

Figure 2.2: Circuit diagram of the source commutated primary converter.

are one of the least reliable parts in the drive system and if one converter bridge fails, the corresponding transformer winding can be disconnected and the train can continue to operate at reduced power. By interleaving the modulation of the inverter legs, the effective switching frequency is increased without increasing the switching frequency of the inverter.

Single phase AC transmission is associated with a significant second order harmonic in the DC-link due to the inherent power pulsation. The second order harmonic is handled by a resonant tank in the DC-link tuned to twice the line frequency. The weight of the second order filter constitutes a significant part of the drive system.

2.2 Direct Conversion

Line side conversion systems based on a source commutated primary converter has been presented in the past [1, 2]. The concept is illustrated in Figure 2.2. The transformer is excited by the VSC and the transformer voltage is utilized to commutate the cycloconverter on the high voltage side. The primary converter can be realized using thyristors but its commutation frequency is limited to a few hundred hertz. Later publications propose the use of self turn-off devices like IGBTs in order to allow higher transformer frequency [4, 10].

The required voltage on the primary side is far beyond the blocking capability of any available switching device. The nominal voltage in Sweden is 15 kV but is usually adjusted to 16,5 kV at the feeder station. However, peak voltages up to 32 kV occur due to severe harmonic distortion [12]. The DC-link voltage is normally limited to approximately half the blocking voltage. Thus, the total required blocking voltage of the primary converter is in the range of 64 kV in a 15 kV system. The blocking voltage of commercially available switching devices is today 6500 V which means that at least ten devices must be connected in series.

Series connection of self commutated devices like the IGBT is a complex task, even though methods to commutate series connected devices exists [13]. Several methods to avoid or simplify series connection have been proposed.

In [10] several converter modules are cascaded as illustrated in Figure 2.3. The voltage across each device in the cycloconverter is clamped by the common DC-link on the secondary side which guaranties correct voltage sharing among the series connected converter structures. With this arrangement it is possible to synthesize a high number of distinct voltage levels at the catenary which reduces the harmonic distortion and simplifies the design of the line filter. However, the converter has to be divided into several separate modules, each containing a primary VSC, Medium Frequency (MF) transformer, and cycloconverter, resulting in a complex insulation system and high component count.

In [4] series connection on the primary side is facilitated by Zero Voltage Switching (ZVS) of the primary converter. During commutation on the high voltage side, the transformer is short circuited by the VSC. By employing ZVS, series connection is simplified at the expense of higher switching losses in the VSC.

The MCC concept was introduced in [6]. By adding capacitive snubbers to the VSC and proper modulation, soft switching can be achieved for all semiconductors in the circuit. In [Publication II] the switching losses on the VSC side were measured in hard and soft switching. It was concluded that the switching frequency could be increased from approximately 500 Hz in

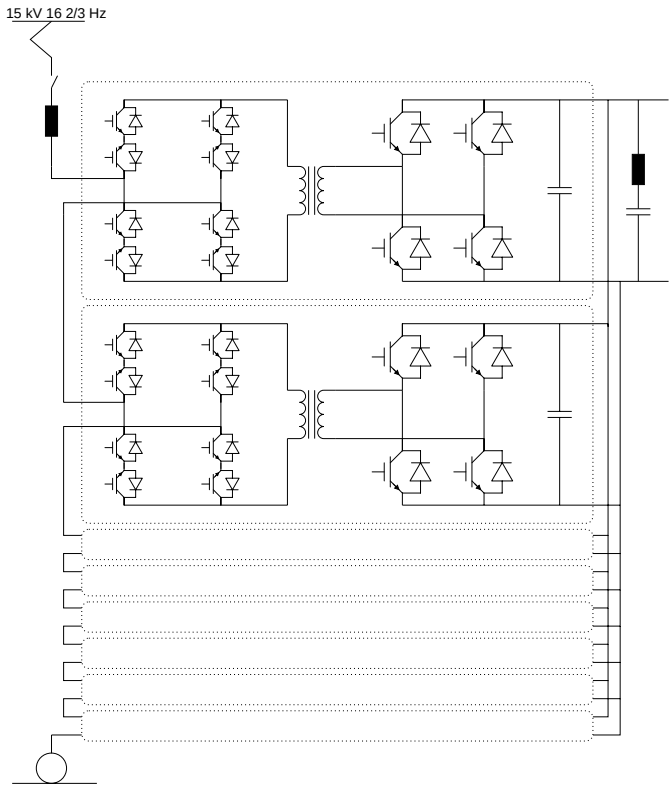

Figure 2.3: Cascaded converter structure with source commutated primary converter.

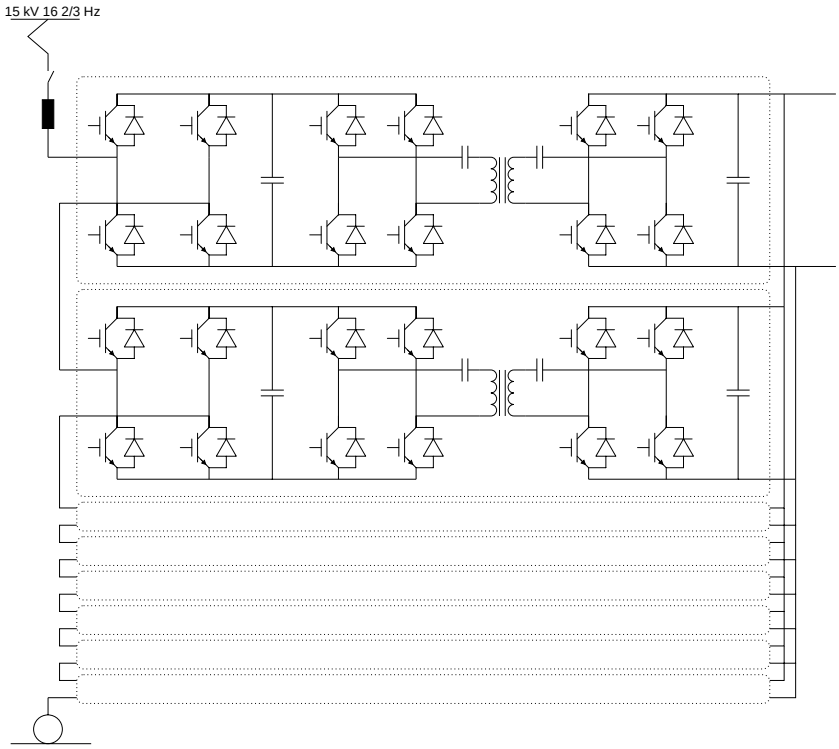

Figure 2.4: Cascaded H-bridge converter structure.

hard switching to approximately 4 kHz in soft switching without decreased efficiency.

2.3 Cascaded H-bridges

A common proposition is to use cascaded H-bridges to synthesize a multilevel voltage at the catenary [7, 9, 11, 14]. The DC-link of each H-bridge is fed by an insulated DC/DC converter comprising a MF transformer. Usually the DC/DC converter employs series resonance in order to achieve Zero Current Switching (ZCS). A common topology is illustrated in Figure 2.4. The series resonant DC/DC converter allows high switching frequency and close coupling of DC-link voltages without any closed loop control [15]. Soft-switching allow switching frequencies in the range of 10 kHz even with

high voltage IGBTs. An efficiency of 97 % has been demonstrated for a resonant DC/DC converter operating at 8 kHz and 2800 V [11].

The MF link can either be a single transformer with multiple primary windings as in [7] or multiple MF transformers with a one to one turn ratio as in [11, 14]. A one to one turn ratio result in a highly modular design as the converters and MF transformer can be packaged together. The same type of IGBT-devices can be used in the primary and secondary converter bridge and the design of the transformer is simplified. Often a coaxial winding arrangement is used [16] which results in low leakage inductance and a simplified insulation system compared to a conventional transformer design. However, the component count is higher compared to a solution with only one transformer and one secondary converter bridge.

The main disadvantage of the cascaded H-bridge topology is the need for a DC-link capacitor at high potential and the lack of soft-switching capability for some of the switches. There is no straight forward way to achieve soft switching of the H-bridge. However, the number of levels is usually high which means that the effective switching frequency seen at the catenary is usually sufficient even with moderate switching frequency of the H-bridge. The modulation of the H-bridge and DC-DC convert is decoupled by the DC-link capacitor and the switching frequency as seen by the catenary can be chosen independently of the transformer frequency.

A high number of cascaded modules can be an advantage for systems operating from multiple voltages. By proper arrangement of the modules, the converter can be reconfigured for multiple AC and DC voltages [9].

2.4 Modular Multilevel Converter

In [8] a traction converter based on the Modular Multilevel Converter (M^2LC) is presented. The M^2LC concept allows a single MF transformer without direct series connected components. Compared to other multilevel converter topologies the M^2LC is highly modular that makes it attractive for high number of levels.

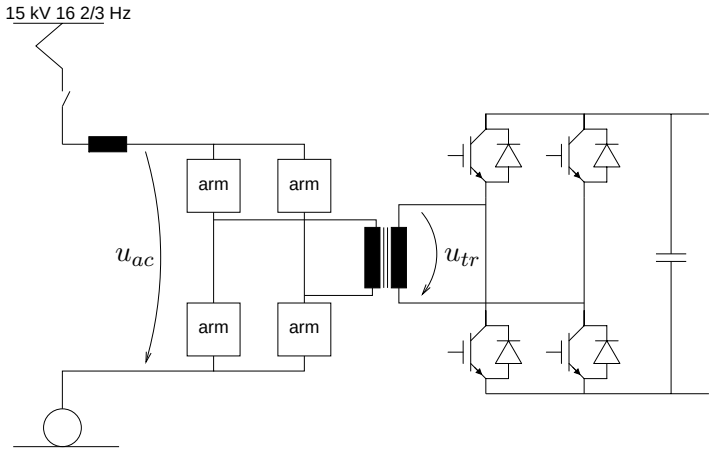

Figure 2.5: Traction converter based on the M^{2}LC concept.

The traction converter based on the M^{2}LC concept is illustrated in Figure 2.5 where each arm consists of $2N + 1$ identical sub-modules according to Figure 2.6. By modulation of the converter arm, an N-level variable voltage can be produced. By varying the converter arm voltages, two independent voltages can be synthesized at the converter terminals. Four quadrant operation is achieved without any external energy transfer to the local storage capacitors.

A drawback of the M^{2}LC is the need for significant amount of energy storage at high potential. According to [8] the required energy storage is approximately 18 J/kVA which is approximately the same as required in the common DC-link of a conventional propulsion system. However, the energy density of the local storage capacitor is smaller than that of the common DC-link and the local storage capacitors add significant weight and volume to the primary converter. Depending on the transformer frequency, the weight of the local storage capacitors may be in the same order of magnitude as the transformer weight.

The M^{2}LC offers full control of the transformer voltage. Thus, the voltage derivative can be limited in order to protect the transformer insulation and avoid emission of electromagnetic disturbances. The fact that only one MF transformer is required result in good power-to-insulation ratio.

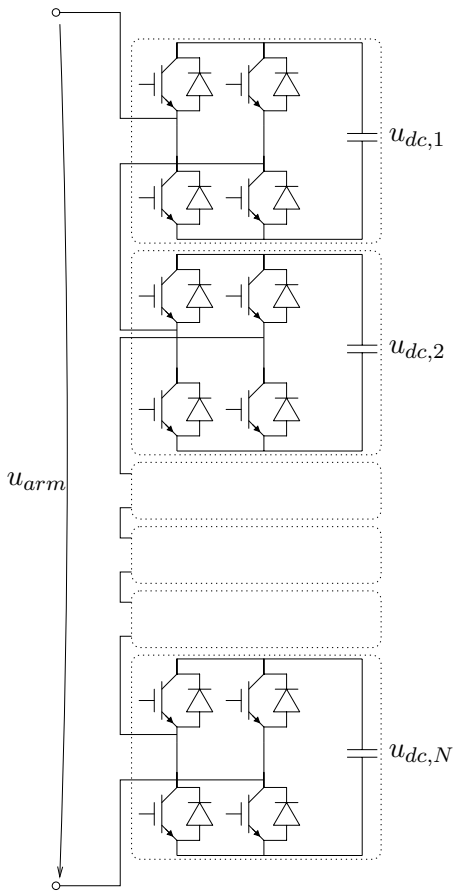

Figure 2.6: Scheme of a converter arm.

2.5 Transformerless Topology

Also topologies without a transformer have been suggested. One such topology, described in [3], is illustrated in Figure 2.7. Instead of having multiple transformers, each module feeds a separate star winding in the traction motor. To increase the DC-link voltage and, hence, reduce the number of levels, the converter cells are realized as a Neutral Point Clamped (NPC) topology.

The slot insulation has to be reinforced to handle the full line voltage. The amount of extra insulation in the traction motor makes it attractive only in high power propulsion systems.

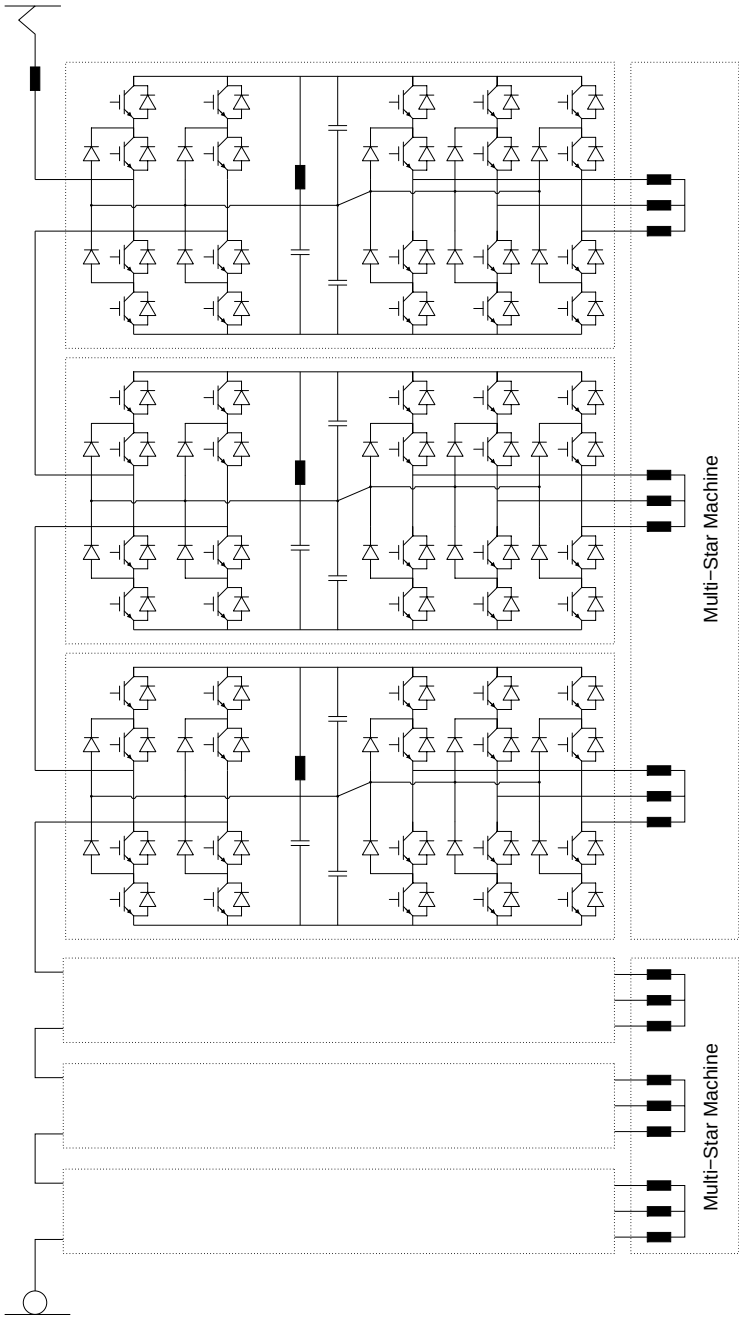

Figure 2.7: Transformerless topology based on cascaded NPC converter feeding separate windings on multi-star machines.

3 Medium Frequency Conversion System

This chapter gives an overview of the studied MF topology. Design issues regarding key components are addressed.

3.1 Topology

The work presented in this thesis is focused on the MCC topology with a limited number of converter cells. Cascading a high number of converter cells has indeed several attractive advantages. A high number of cascaded cells allow synthesis of a high number of voltages at the AC terminal which allows smaller line filter. The series connection of components can be completely avoided with a sufficiently high number of converter modules and the transformer design is simplified as the voltage stress at the switching frequency is decreased. However, the cascaded approach inevitably results in high component count and complex insulation between modules. Resent investigations [7, 10, 11] on cascaded topologies report minimal volume reduction and 30% to 50% weight saving on the system level even though the weight of the MF transformer in some cases is as low as 0,1 kg/kVA. Therefore, efforts have been made to simplify the primary converter stage. Parallels can be made to VSC based High Voltage Direct Current (HVDC) transmission introduced in 1997 [13]. The converter bridge is a hard switched six-pulse, two-level converter with series connected IGBTs in each valve. The upper range for ABB's VSC-based HVDC transmission (HVDC Light) is today $\pm 320\,\mathrm{kV}$ and 1200 MW.

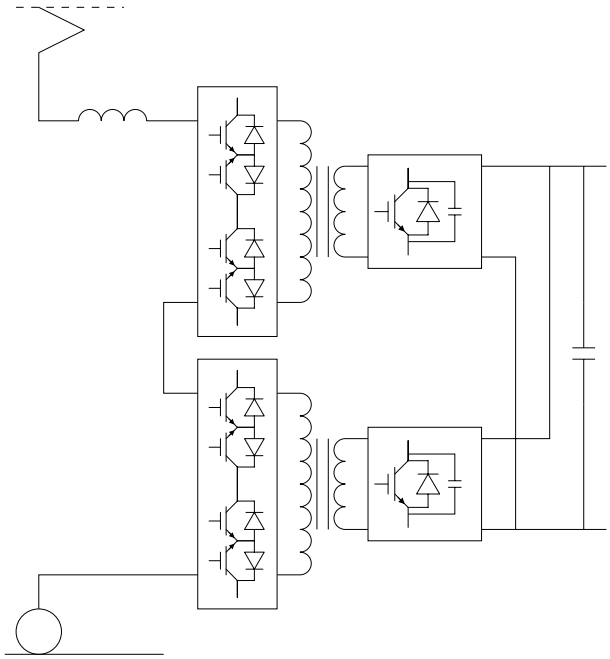

Figure 3.1: Proposed topology for EMU applications.

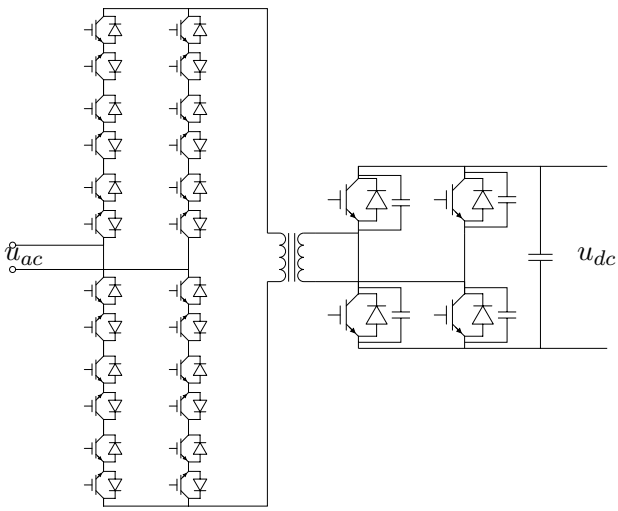

Figure 3.2: Circuit diagram if the studied converter cell.

Choosing the appropriate number of levels is a compromise between the voltage stress on the insulation of the line filter and the transformer on one hand and the complexity on the system level on the other hand. A solution with only two converter cells, depicted in Figure 3.1, is an attractive compromise. Five level output is provided at the AC terminals and the MF stress on the transformer winding and line side filter is reduced by half compared to a solution with a single converter cell. The proposed solution is very similar to the conventional system illustrated in Figure 2.1. Synergy with the conventional drive system is important as the MF transformer will, at least in the beginning, only be a viable alternative in certain niche products. Figure 3.2 shows the basic converter cell of the studied topology.

3.2 Voltage Source Converter

Current state-of-art traction converters are highly modularized and the same type of converter structure and mechanical design is used for line converters, auxiliary converters and AC motor drives. The studied dual bridge configuration is well suited to this philosophy. The same converter structure is reused with modification only in software and, if ZVS is required, capacitive snubbers. Thus, the studied configuration share a higher number of components with the state-of-the-art solution compared to cascaded solutions or the transformer less solution.

In [Publication II] a loss model of the conventional VSC as well as the new primary switched converter structure is presented. It is concluded that the switching frequency can be increased beyond 4 kHz without derating of the converter during motoring. The current handling capability of the investigated module, which is optimized for hard switched applications, is fairly independent of the direction of the power due to good balance between diode and IGBT chips. However, the distribution becomes worse when soft switching is applied. The current has to be decreased by approximately 25% at 4 kHz during regenerative braking. This constitutes no problem as necessary braking torque is normally lower than motoring torque. The switching frequency can be increased beyond 2 kHz even if the

capacitive snubbers are excluded, mainly due to eliminated reverse recovery loss. Therefore, an MF system with no modification to the VSC is viable.

3.3 Medium Frequency Transformer

3.3.1 Transformer Fundamentals

The transformer is used to transfer energy between to circuits that are magnetically coupled. The transformer provides a mean to galvanically isolate two or more circuits and to adapt to different voltage and current magnitudes. The size and weight of the transformer is heavily dependent on the transformer frequency.

The relationship between the voltage and flux is given by Faraday's law of induction.

$$e(t) = N\frac{d\phi(t)}{dt} \tag{3.1}$$

Thus, the transformer flux can be found by integrating the applied voltage.

$$\phi(t) = \int_0^t \frac{e(t')}{N} dt' \tag{3.2}$$

Assuming square wave excitation the peak flux becomes

$$\hat{\phi} = \frac{U_d}{4 f_{tr} N}. \tag{3.3}$$

For a certain peak flux density, the necessary core area can be calculated.

$$A_c = \frac{\hat{\phi}}{\hat{B}} \tag{3.4}$$

The current loading is determined with respect to cooling conditions according to

$$NI = A_w f_w J. \tag{3.5}$$

Thus, the size of the transformer is given by the product

$$A_c A_w = \frac{U_d I}{4 f_{tr} J f_w \hat{B}}. \tag{3.6}$$

By increasing the excitation frequency, the size of the transformer can be reduced considerably. However, the amount of insulation does not decrease at the same rate as the amount of copper. The reduced fill factor at elevated frequencies diminishes the reduction of the transformer size and the design of the high voltage insulation becomes critical.

Interleaving the windings is an efficient mean of lowering the leakage inductance. Low leakage inductance is necessary to achieve low commutation losses in the primary converter. If the leakage flux is assumed to flow only in the high voltage insulation, the leakage inductance becomes

$$L_k \approx \mu_0 \frac{P N^2}{n h} g_1 \tag{3.7}$$

where n is the degree of interleaving, P is the mean-turn-length, N is the number of turns, g_1 is the primary insulation thickness, and h is the height of the winding. However, interleaving the high voltage winding increase the complexity of the transformer and the fill factor decrease as the amount of insulation increase. Therefore, only the low voltage winding is interleaved, see Figure 3.3, and the leakage inductance of the transformer becomes

$$L_k = \mu_0 \frac{P N^2}{4 h} \left(\frac{t_1 + t_2}{3} + 2 g_1 \right) \tag{3.8}$$

where t_1 and t_2 is the thickness of the winding layers.

3.3.2 Core Material

Laminated silicon steel has been the first choice for power transformers for a long time. It is sold at a low price and is available in large sheets in large quantities. Only if the design is not feasible in standard magnetic steel, should more exotic materials be investigated.

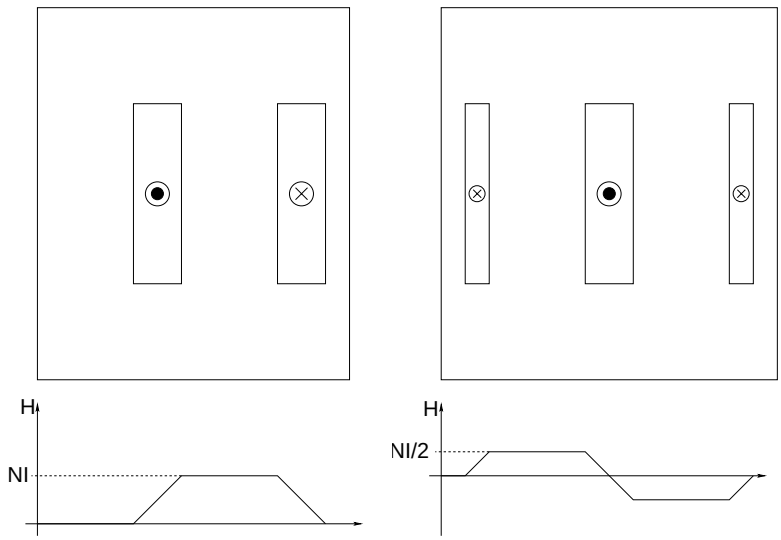

(a) Non-interleaved winding (b) Interleaved low voltage winding

Figure 3.3: Effect of interleaving.

Core losses are dominated by hysteresis losses and eddy current losses. Hysteresis losses are the energy consumed to align the magnetic particles of the steel with the magnetic field. The hysteresis loss can be found from the area of the BH-loop.

$$W_h = \oint H \cdot dB \tag{3.9}$$

The hysteresis losses are, hence, proportional to the excitation frequency. Steinmetz's equation gives an approximation of the area of the hysteresis loop.

$$p_h = f_{tr} k_h \hat{B}^{\beta} \tag{3.10}$$

At higher frequencies eddy current losses often become dominant. As long as the lamination gauge is significantly lower than the skin depth, eddy current losses are proportional to the square of the excitation frequency.

$$p_e = k_e f_{tr}^2 \tag{3.11}$$

For thicker lamination, flux distribution is non-uniform, thus increasing the effective permeability.

Normally, all losses are summarized and expressed as the specific core loss.

$$p_c = K_1 f_{tr}^{K_2} \hat{B}^{K_3} \tag{3.12}$$

The specific core losses are normally given in the datasheet for sinusoidal excitation. However, they can easily be determined for square wave excitation. For more complex flux waveforms the modified Steinmetz's equation can be used to take non sinusoidal flux into account.

Eddy current losses are caused by circulating currents induced by the varying magnetic field. Eddy current losses can be reduced by shortening the current path and by increasing the resistivity of the magnetic material. Reducing the current path is done by decreasing the lamination thickness and the resistivity is controlled by additives in the alloy, usually silicon.

The resistivity can be increased and magnetostriction can be reduced by increasing the amount of silicon, and the optimum amount of silicon with respect to magnetostriction is 6,5%. However, manufacturing high-silicon steel (above $3,5\%$) by conventional cold rolling methods is difficult as the material becomes hard and brittle. One way of producing steel with high silicon content is to diffuse silicon into the sheet after the cold rolling process [17].

Amorphous metals are formed by rapid solidification of the melt [18]. At cooling rates above $10^6\,\mathrm{K/s}$, the alloys form a glass-like structure without a periodic crystalline arrangement of the atoms. Due to the production technology, these alloys are only available in thin metal strips. Typical thickness is $20\,\mu\mathrm{m}$ and the strip width is in the order of $250\,\mathrm{mm}$.

The glass-like structure makes the amorphous alloys brittle and the material must be carefully handled and protected from shocks during service. The mechanical properties also make it hard to machine the material and the practically realizable structures are limited. The most convenient structures are the toroidal or stadium shaped wound cores with an optional cut. The amorphous materials are also sensitive to thermal aging. During service, the maximum temperature may have to be limited to $80\,^\circ\mathrm{C}$. The saturation flux is also reduced in an amorphous alloy. This is due to the non-crystalline structure of the material.

The dominating amorphous alloys are either cobalt or iron based. The iron based alloys have significantly higher saturation flux compared to the cobalt based, but suffer from high magnetostriction. For the iron based alloys, saturation flux may be above 1,4 T, but magnetostriction may be as high as 30 ppm, causing significant coercivity and high noise levels. The cobalt base alloys can have zero magnetostriction, but saturation flux may be as low as 0,5 T - 0,8 T.

It has been found that heat treatment of some glasses would form ultrafine crystalline structures of about $10 - 15$ nm embedded in an amorphous matrix. These nanocrystalline iron based materials have improved saturation flux compared to the cobalt based amorphous alloys, but significantly lower magnetostriction. Near zero magnetostriction is achieved by controlling the annealing temperature and silicon content. The crystalline structures have negative magnetostriction, while the magnetostriction of the residual amorphous content is highly positive. With proper annealing, the amount of residual amorphous content can be controlled, resulting in zero over all magnetostriction. The nanocrystalline materials also have superior temperature stability compared to the amorphous alloys.

During the annealing of the nanocrystalline material, it becomes extremely brittle. After formation of the nanocrystalline structure, further machining of the core is impossible and the core must be handled with care during assembly of the end product and during service.

Figure 3.4 illustrate specific core loss at 4 kHz for two amorphous materials and one nanocrystalline material according to the manufacturer's datasheet. The amorphous material 2605SA1 from Metglas is iron based and has significant higher losses compared to the cobalt based amorphous VITROVAC 6030 F from Vacuumschmelze. The iron based nanocrystalline VITROPERM 500 F has lower losses than the amorphous VITROVAC 6030 F and also significantly higher saturation flux density.

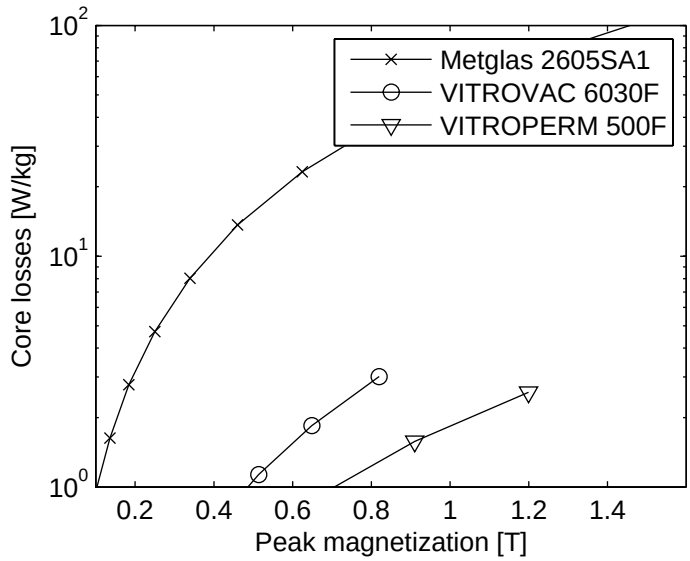

Figure 3.4: Specific core loss at 4kHz sinusoidal excitation for a number of available amorphous and nanocrystalline materials.

3.3.3 The Transformer Geometry

The loss density in the core is inevitably higher in the MF transformer compared to the conventional traction transformer. Even though the efficiency of the transformer becomes high due to its small size, efficient cooling of the core is an essential design constraint. From Figure 3.4 it can be concluded that the loss density in the core varies between $10-100\,\mathrm{W/kg}$, which is ten to hundred times higher than the loss density in a conventional transformer. Therefore, direct water cooling of the core is preferable.

The transformer geometry must be adapted to the available core shapes. For thin laminated steel, like the amorphous and nanocrystalline materials as well as conventional thin steel, wound cores are the cheapest to manufacture even thought other laminations are available. Therefore, the toroid and C-core are preferable.

A coaxial winding arrangement results in low leakage inductance and uniform voltage stress on the insulation. Thus, the coaxial transformer has

high utilization of the insulating material. However, the fill factor is poor and it is difficult to construct a transformer with high turn-ratio. Low leakage inductance is a prerequisite for low reverse recovery losses. However, some inductance simplifies commutation of the MCC. Especially during low load where resonant commutation is used.

Cooling of the winding can be achieved by means of cooling ducts in the high voltage insulation. However, the voltage handling capability of the insulation is reduced by the presence of an oil duct. The permittivity of oil is lower than that of paper and, thus, a mayor part of the voltage will appear across the duct. The permissible field strength in the oil is also lower than that of the paper.

Steep voltage flanks and increased operating frequency are known to cause hot-spots and life time reduction. To predict the transformer behaviour under these conditions the capacitance of the transformer windings must be considered. There is capacitance present between transformer windings and grounded parts, turn to turn, and layer to layer. Due to the capacitance, the voltage distribution across the winding turns during steep voltage flanks will not be uniform, and uneven voltage distribution may cause hot-spots and inter-turn insulation breakdown. The inter-turn voltage may be controlled either by modifying the parasitic capacitance or, if necessary, reducing the voltage flanks.

The proposed transformer topology is illustrated in Figure 3.5. The winding is prefabricated and the C-shaped cores are clamped around the winding by water cooled plates. To limit the amount of insulating material in the winding, the HV winding is a single layer winding made from Litz-wire. There is no direct cooling of the HV winding and losses in the winding have to be transported by conduction through the HV insulation.

The proposed transformer topology is suited both for dry and oil immersed designs. Dry insulation is preferable since very high hot spot temperature can be allowed. However, the dielectric losses can cause problems with dry insulation. The dissipation factor is several orders of magnitude higher for available dry insulating materials compared to conventional combination of

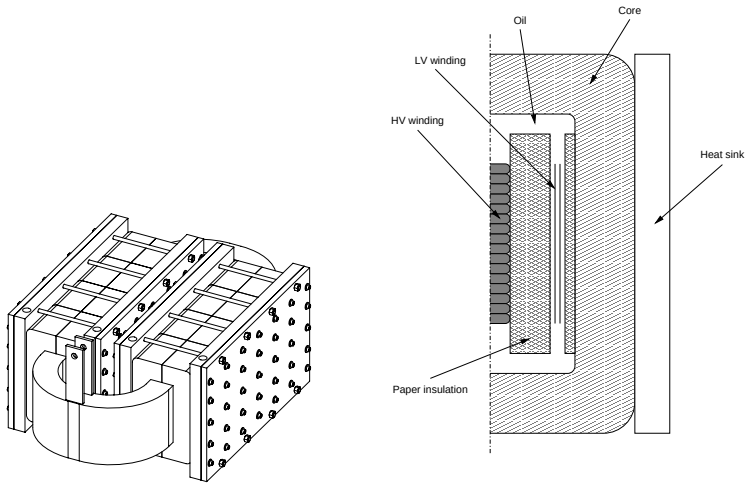

(a) Perspective view (b) Cross section

Figure 3.5: Studied transformer topology

oil and paper. Therefore, heating due to dielectric losses in the insulating material should be considered for a dry design.

3.3.4 Optimization of the Transformer

The transformer geometry has been optimized using a numerical optimization tool [Publication I]. The most important design parameters are listed in Table 3.1. The rating of the transformer is suitable for a transformer in a dual bridge configuration, according to Figure 3.1, in a typical EMU application. The transformer has been optimized solely on weight of the transformer. However, certain other design aspects can be incorporated as constraints.

The minimum transformer weight was investigated for two different core materials. One conventional non-oriented silicon steel and one amorphous material. Figure 3.6 and Figure 3.7 show the minimum transformer weight as a function of leakage inductance and frequency. From the figures, it is clear that the transformer design is only appropriate for high frequencies.

Table 3.1: Selected design parameters

Property	Symbol	Value
Rated power	S_n	600 kW
Rated voltage	U_n	7,5 kV
DC-link voltage	U_d	1800 V
Peak flux density	$\hat{B}$	< 1 T
Temperature rise	θ	55 K
Primary insulation thickness	g_1	12 mm
Secondary insulation thickness	g_2	2 mm
Strand diameter	d_{st}	0,2 mm
Fill factor	f_w	0,75

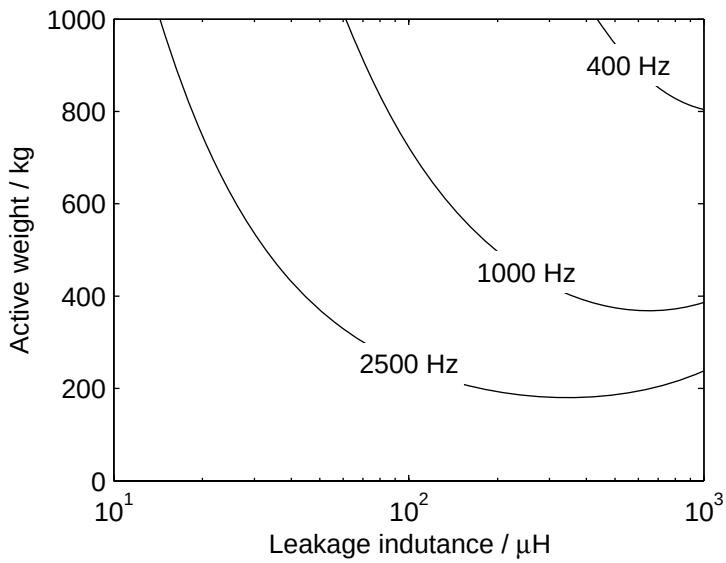

Figure 3.6: Minimum transformer weight as a function of leakage inductance and operating frequency using Sura NO10.

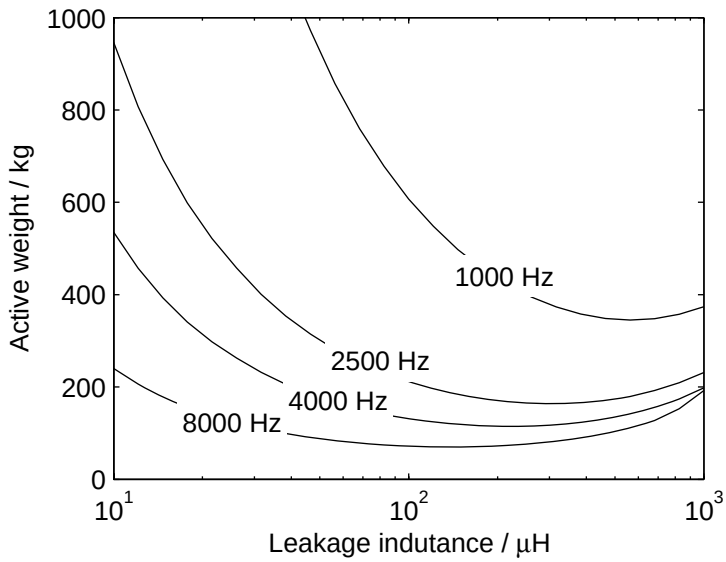

Figure 3.7: Minimum transformer weight as a function of leakage inductance and operating frequency using Metglas 2605SA1.

The choice of transformer structure was made under the assumption that the insulation to power ratio is high. For lower frequencies or higher power rating direct cooling of the HV winding is preferable. The relationship between leakage inductance and transformer weight is fairly loose in the range which is suitable for commutation of the primary converter. Hence, the leakage inductance can be chosen freely with respect to the commutation.

Three different transformer designs have been compared and the result is listed in Table 3.2. The first design is based on an amorphous core operated at four kilohertz which has been found to be a suitable frequency for the voltage source converter. The weight of the transformer is slightly higher than the minimum value in Figure 3.7 due to an additional constraint in the optimization procedure that require an efficiency above 99%. The weight penalty for doing so is very small compared to optimizing purely on weight. The second design is also based on an amorphous core but operated at eight kilohertz. The peak magnetization flux has to be reduced significantly to fulfill the efficiency requirement and, thus, the weight reduction compared

Transformer	1	2	3
Material	Metglas 2605SA1	Metglas 2605SA1	Sura NO10
Ribbon thickness	25 µm	25 µm	100 µm
Magnetization frequency	4000 Hz	8000 Hz	2500 Hz
Active weight	136 kg	101 kg	205 kg
Efficiency	99%	99%	98%
Peak magnetization	0,99 T	0,66 T	0,85 T
Core losses	52 W/kg	75 W/kg	88 W/kg
Leakage inductance	100 µH	100 µH	400 µH
Power density	0,23 kg/kVA	0,17 kg/kVA	0,34 kg/kVA

Table 3.2: Comparison of three different transformer designs.

to the four kilohertz transformer is small. However, increasing the frequency significantly decrease the audible magnetic noise. The third design is based on conventional electric steel and, hence, operates at a lower frequency (2500 Hz). The efficiency requirement had to be decreased to 98% in order to acquire a reasonable design.

3.4 Cycloconverter

As mentioned in Section 2.2, the blocking voltage of the primary converter is in the range of 64 kV and, consequently, several switches have to be connected in series. Since the typical power rating of a typical EMU is approximately 1 MVA per converter module, the current is typically 66 A.

The cycloconverter is made up from a string of subvalves connected in series. Each subvalve contains power devices, gate drivers, communication interface, power supply, and protection. The valve has to be integrated in a way that makes it suitable for series connection.

3.4.1 Switching Device

The maximum blocking voltage of commercially available IGBTs is 6500 V. However, the optimum blocking voltage may be lower due to the ratio between conduction losses and switching losses.

The losses in the primary converter are dominated by conduction losses and reverse recovery losses. The losses during reverse recovery are related to the magnetic energy stored in the transformer during reverse recovery.

$$W_{rr} = \frac{1}{2} L_k I_{rr}^2 \tag{3.13}$$

The peak reverse recovery current is assumed to be proportional to the square root of the current slope if the reverse recovery is assumed to be snappy and the commutation time is lower than the carrier lifetime. The current slope is inversely proportional to the commutation inductance. Thus,

$$I_{rr} \propto \sqrt{\frac{1}{L_k}}. \tag{3.14}$$

Combining (3.13) and (3.14) yields that the magnetic energy stored in the transformer during reverse recovery is approximately independent of the commutation inductance. The reverse recovery current at reduced commutation speed was measured in [19]. The peak reverse recovery current for an Ixys DH60-18A diode is given in Figure 3.8. The agreement between the measured peak reverse recovery and the predicted value according to (3.14) is satisfactory.

The relationship between on-state voltage and switching losses is given by the so called trade-off curve. A bipolar device, such as the IGBT or PiN-diode, can be optimized for different switching frequencies by controlling the carrier lifetime and thus move along the trade-off curve. The trade-off curve is unique for each technology. Up to now, the dominating technology for high voltage components is the Non-Punch Through (NPT). However, new structures like the Punch Through (PT), Soft Punch Through (SPT) are emerging even for 6500 V devices.

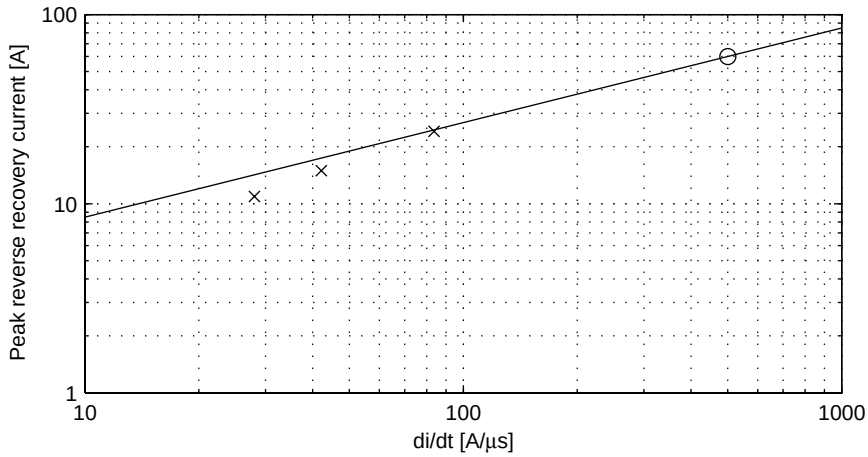

Figure 3.8: Reverse recovery current as a function of commutation speed. Sample point given in data sheet (ring), Expected reverse recovery behaviour according to Equation 3.14 (solid), and samples at reduced commutation speed.

Choosing the power devices for a certain application is a problem with many degrees of freedom. However, a simple comparison between diodes with different blocking voltage and different current rating can be made according to

$$f(k, f_s) = \frac{\frac{k \cdot f_s \cdot E_{rec}}{I_F} + U_F}{U_{RRM}}, \tag{3.15}$$

where f_s is the switching frequency and k is a factor to take external losses in for example snubbers into account. Equation 3.15 is evaluated in Figure 3.9 for a number of commercially available diodes. The switching frequency is assumed to be 4 kHz and $k = 2$ corresponding to one commutation per halfcycle and no external losses (snubberless). This comparison penalizes low voltage components as snubber losses will be considerable in reality. Even though the comparison is coarse, some conclusions can be made. Firstly, the diode losses are dominated by the reverse recovery losses and, hence, the lowest blocking voltage is most favourable in terms of loss at the investigated frequency. Secondly, the sign of the slope depends on die generation and optimization. For the older ABB SPT dies, there is a strong positive correlation between losses and blocking voltage, while there is a negative correlation for the more modern ABB SPT+. The NPT dies from

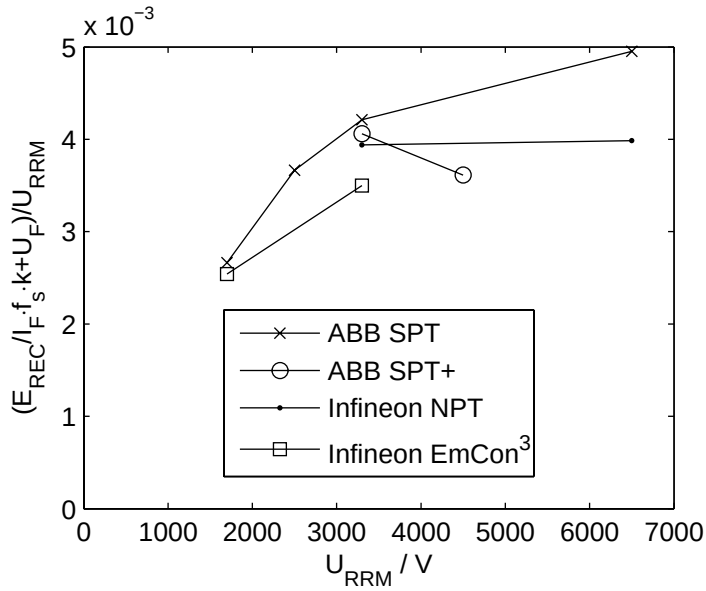

Figure 3.9: Diode loss comparison for different blocking voltages.

Infineon are probably optimized for a higher switching frequency compared to the ABB dies and the dependency on blocking voltage is almost zero. A similar investigation can be made for the IGBT, but the switching losses cannot be easily determined from datasheets in case of soft-switching. However, the voltage drop across the IGBT can be added to the diode forward voltage and compared to the recovery losses but the ratio between IGBT and diode dies has to be determined. To conclude, there is no clear optimum blocking voltage regarding losses. Instead, the main switching device can be selected from a valve integration point of view.

3.4.2 Snubber Circuit

The purpose of the snubber circuit is to:

- Protect the valves from the magnetic energy stored in the transformer during reverse recovery.

- Ensure proper static and dynamic voltage sharing across series connected components.
- Limit Electro Magnetic Interference (EMI) during switching.
- Recover energy from the main circuit for gate drive power supplies.
- Protect the cycloconverter during fault.

Many possible snubber arrangements are listed in literature. However, some of the most common are shown in Figure 3.10.

Limiting the diode voltage during reverse recovery can be accomplished by an RC snubber (Figure 3.10a). However, recharging of the RC snubber cause significant losses at low load. In [20] it was found that the cycloconverter snubbers reduce the efficiency by 2% in a particular case. Losses occur, not only during reverse recovery of the protected diode, but also during commutation in the other cycloconverter legs and during transformer voltage reversal. The choice of an optimum RC snubber is addressed in [21].

One way to reduce the losses associated with the RC snubber, especially at low load conditions, is to use a clamping circuit (Figure 3.10b). In this circuit, the voltage is clamped to an approximately constant level given by the capacitor voltage. The losses are reduced especially at low load. However, the size of the clamping capacitor is significantly larger compared to the RC snubber capacitor. The size of the clamping capacitor may have a significant influence on the valve integration.

Selecting the clamping voltage is a trade off between maximum tolerable voltage and losses. Assuming a constant clamping voltage, i. e. active clamping or large clamping capacitor, the energy transferred to the snubber becomes

$$W_c = \left(1 + \frac{1}{\frac{U_c}{U_d} - 1}\right) W_{rr} \tag{3.16}$$

where U_c is the clamping voltage.

[Publication IV] presents a method to utilize the antiparallel IGBT to limit the voltage across the diode during reverse recovery. The IGBT is used in its

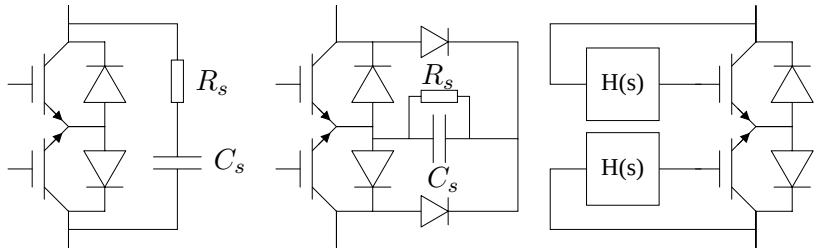

(a) RC snubber (b) Clamping snubber (c) Active snubber

Figure 3.10: Possible snubber arrangements

linear region to limit the voltage across the diode to a preset level (Figure 3.10c). The snubber losses are the same as for the RCD-snubber if the clamping voltage is equal but the bulky snubber capacitor is avoided since the energy is dissipated instantaneously in the IGBT.

The active snubber scheme does not necessarily imply over rating of the IGBT. One IGBT contribute to the current conduction only for one half of the fundamental cycle depending on the direction of the current. The same IGBT act as snubber for the second half of the fundamental cycle. Thus, active snubbing may result in a more even loss dissipation during the fundamental cycle and, hence, lower temperature swing at the chip. Therefore, active snubbing may even result in better reliability due to less power cycling.

3.4.3 Energy Recovery

Power to the valve is provided either from ground potential via an isolated DC/DC converter or by tapping energy from the main circuit. The valve is subjected to voltage derivatives higher than 30 kV/µs and peak voltages in excess of 50 kV to ground. The nature of the voltage stress makes it difficult to supply the gate driver from ground and an attractive alternative is to pickup the necessary energy from the main circuit. Harvesting energy from the main circuit can be done by leaking current when the valve is in its off-state, shunting current from the main circuit when the device is in its on state, or recover energy from the snubber circuit.

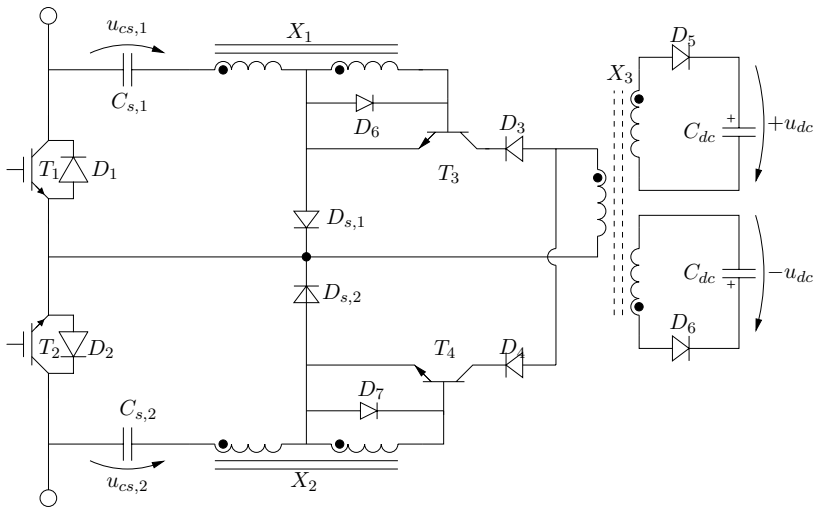

Figure 3.11: Snubber energy recovery circuit

In [22] a method is presented to use energy recovered from the turn-off snubbers to power a Gate Turn-off Thyristor (GTO) gate drive. The energy recovery circuit has been adapted to the bidirectional valve. The modified gate driver is shown in Figure 3.11.

The valve is equipped with a small passive turn-off snubber. The size of the snubber can be very small since it only has to limit the voltage derivative during reverse recovery due to the active clamping mechanism. The energy transferred to the snubber capacitor can be recovered and used to power the gate driver.

The operation principle of the recovery circuit is as follows. The energy transferred to the snubber capacitor during reverse recovery is recovered during the turn-on of the IGBT. During turn on of transistor T_1 a resonant path is formed by the snubber capacitor C_{s1} and the leakage inductance of transformer X_3 via the diode D_3 and transistor T_3. Base current to transistor T_3 is provided via the current transformer X_1. Meanwhile, the diode D_4 blocks the current path through capacitor C_{s2}. When the snubber capacitor C_{s1} is emptied, the diode D_{s1} is forward biased and transistor T_3 is turned off causing the current to commutate to diode D_5. A similar process can be described for turn on of transistor T_2,

The rating of transistors T_3 and T_4 are determined by the required power transfer and is independent of the voltage and current rating of the main switch. The transistors are only switched off when the snubber capacitor is fully discharged and the snubber diodes are forward biased. Therefore, the transistor has to block only the unregulated DC voltage transformed by the transformer X_3 and sustain the peak current determined by the impedance of the resonant circuit formed by the snubber capacitor and the magnetizing inductance of the transformer X_3. The ratio between blocking voltage and peak current can be chosen freely by varying the turn ratio of the transformer X_3.

In the following paragraphs, the amount of energy harvested from the snubber circuit is derived. For simplicity, overvoltages occurring during transitions are neglected. They can easilly be accounted for but the contribution to energy transfer is minimal.

Turn-off Prior to the turn-off, both snubber capacitors C_{s1}, and C_{s2} are empty. During reverse recovery a resonant current path is formed by the leakage inductance of the transformer and the snubber capacitor C_{s1} and snubber diode D_{s1} or capacitor C_{s2} and snubber diode D_{s2} depending on the direction of the current. The snubber capacitor that is a part of the resonant circuit is charged to the the nominal voltage U_d. The other capacitor remains uncharged and there is no energy transfer.

$$W_{off} = 0$$

Voltage reversal During the voltage reversal a resonant path is formed through both snubber capacitors in series, the leakage inductance of the transformer X_3 and the supply. As the voltage across the previously charged snubber capacitor reach zero, the current is commutated to the DC storage capacitor. Assuming that the duration of the voltage reversal is significantly shorter than the time constant of the resonant circuit, the transferred energy is

$$W_{rev} = C_s U_d^2. \tag{3.17}$$

Turn-on During turn-on both snubber capacitors are fully discharged and the energy is transferred to the storage capacitor.

$$W_{on} = \frac{1}{2} C_s U_d^2 \tag{3.18}$$

Total recovered energy The total energy recovered can be found by summing (3.17) and (3.18) and multiplying by the transformer frequency.

$$P_{supply} = 3 f_{tr} \frac{C_s U_d^2}{2}. \tag{3.19}$$

Initialization The subvalve power supplies can be initialized without any auxiliary circuit provided that the DC-link can be charged by other means, and that the subvalves are able to support voltage without power. It is assumed that enough energy, to charge the DC-link and initialize the primary converter, can be supplied by the on-board battery.

During initialization there is no energy to turn on the main transistors. However, the resonant current path can be closed through the transformer and the voltage source converter. The transformer voltage is shared between all subvalves. Thus, the voltage across each valve is only half of the nominal voltage. Since the energy transfer is proportional to the square of the voltage across the valve, the transferred energy during each voltage reversal is only one forth compared to a voltage reversal during operation.

$$W_{rev,init} = \frac{1}{4} W_{rev} \tag{3.20}$$

However, each valve will be subject to two voltage reversals each cycle. Thus, the recovered energy during initialization becomes

$$P_{init} = f_{tr} \frac{1}{2} C_s U_d^2. \tag{3.21}$$

Accordingly, the recovered power during initialization is one third of the recovered energy during normal operation. Enough power to initialize the gate drivers can be supplied by temporally increasing the transformer fre-

quency. This constitutes a minor problem as the load current is zero. However, the capacitive snubbers must be considered since the VSC must be hard switched.

3.4.4 Signalling

Each valve position requires a multitude of command and feedback signals. The valve receives gate signals for both channels and sends information about the switching state and error signals back to the modulator. To allow small snubber circuits, it is essential to guarantee precise timing of the series connected valves.

High voltage insulation is usually provided by optical components or magnetic components. Optical components may be either optocuplers providing moderate insulation voltage or fibre optics providing very high insulation voltage over large distance. Optocuplers and fibre optics are associated with rather high propagation delay time. Typical values are from 40 ns up to hundreds of micro seconds. Magnetic components used to provide high voltage insulation are usually pulse transformers. Pulse transformers provide moderate insulation voltage and very low propagation delay. The rise time is typically in the order of a few nanoseconds. An alternative to pulse transformers are magnetoresisitive isolators. These devices are integrated circuits containing a coil and a magnetoresistive sensor. By applying a short current pulse to the coil, the transducer is forced in one of two remanent states. Since current only flow during transition, power consumption on the sending side is very low and comparable to opto isolators on the receiving side. The propagation delay is typically ten nanoseconds and the maximum data rate is 100 Mbaud.

If a very high insulation voltage is provided, for example by a fibre optic link, there may be a direct link between the modulator and the subvalve position or, if only moderate insulation is provided, the subvalves may be daisy-chained (see Figure 3.12). Paralleling of the communication provide low latency and less strict requirements on propagation delay. However, the high insulation requirements probably rule out all forms of communication but fibre optics. Daisy-chaining reduce the number of channels by half,

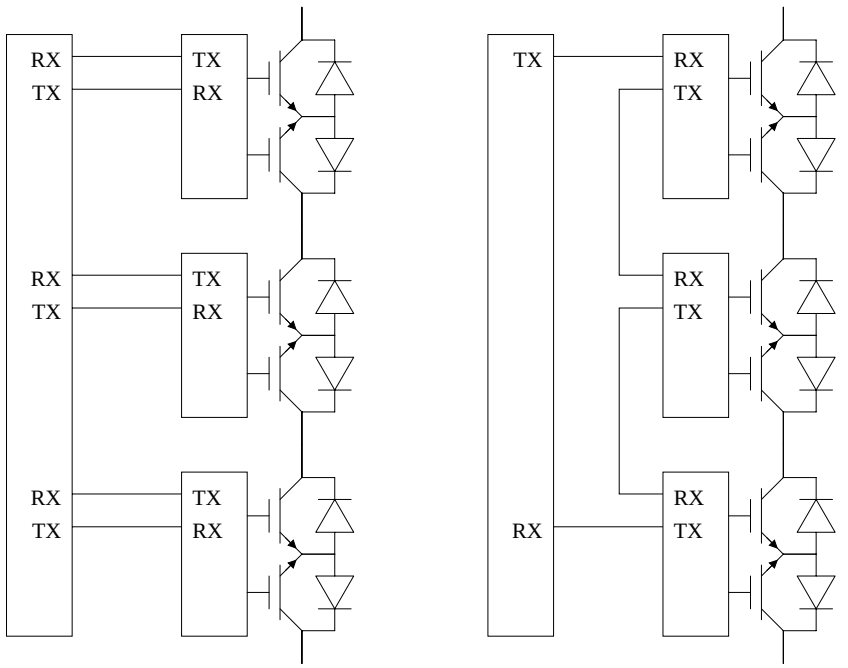

Figure 3.12: Parallel communication (left) and daisy chained communication (right)

and also reduce the communication distance by only connecting to adjacent positions. Also, the insulation requirements are lower then for paralleling. Since turn-on must be very precisely coordinated among positions, there are strict requirements on predictability of the propagation delay. Also, the command latency will become large if a larger number of positions are daisy-chained. Possibly, only a few positions are daisy-chained, forming a sub module, in turn connected in parallel to the modulator.

A local clock must be maintained at each valve position. The clock might be distributed over the communication link, synchronizing all positions, or it might be a free running clock. Non synchronized system clocks will result in turn-on uncertainty equal to the system clock period. However, if clocks are synchronized the turn-on uncertainty is equal to the jitter in the local clock.

A clock can be distributed separately from the data stream or embedded into it. Embedding the clock into the data stream allow for a single data channel for both clock and data and is therefore favourable if a relatively costly media like fibre optics is used, but additional clock recovery circuitry must be implemented at the position.

3.4.5 Reliability and Lifetime

Failure rates are often expressed as the expected number of failures during a specific duration of time. One common measure is the Failure in Time (FIT) rate which is the number of expected failures during one billion hours of operation.

The FIT rate is normally additive. Thus, the FIT rate for an apparatus is assumed to be the sum of the FIT rate for each component in the apparatus. This is true if there is no redundancy and the failure processes are independent.

Two important failure mechanisms in power semiconductors are solder fatigue and bond wire lift off. Solder fatigue is the result of the mechanical stress due to the thermal cycling of the bimetallic interface between the ceramic and the base plate. The wear results in higher thermal resistance and the damage from thermal cycling is reduced in traction grade modules by replacing the common Cu baseplate by another material (AlSiC) with a thermal expansion coefficient closer to that of the ceramic. Bond wire lift off is caused by the bending of the bond wire due to varying temperature of the chip. These variations are caused by low output frequency (power cycling). Bond wire lift off cause an increase of the on-state voltage of the component. Traction grade modules have improved bonding compared to standard modules.

The damage caused by solder fatigue and bond wire lift off is considered accumulative and the number of cycles to failure is given by the Coffin-Manson law. The number of cycles to failure for a certain temperature cycle ΔT is given by

$$N_f = \frac{Q}{(\Delta T)^{\gamma}} \tag{3.22}$$

where Q and γ are constants that are generally determined from accelerated tests. Lifetime is calculated assuming linear accumulation of damage, i. e. a wear function is defined,

$$F = \sum_{k=1}^{i} \frac{1}{N_f\left(\Delta T_k\right)}, \tag{3.23}$$

and failure occur as $F = 1$.

A string of series connected components are subjected to the same stress and, thus, subjected to the same damage. The string of components will fail at approximately the same time, according to the Coffin-Manson law. Therefore, FIT analysis is not a proper way to predict failure due to thermal cycling.

3.4.6 Redundancy

The reliability of the conversion system is inherently lower compared to the conventional system and efforts must be made to keep the availability of the system high. This is accomplished by some form of redundancy. Electric railway vehicles are normally not equipped with fully redundant converters. Instead several converters are operated in parallel connected to separate transformer windings. Thus, in case of a faulty converter module, it can be disconnected and the train can continue to operate at reduced power.

3.4.6.1 Bypass switch

Redundancy can be achieved by means of a bypass switch across each sub-valve. A faulty valve may then be short-circuited by the switch and the voltage is redistributed across the remaining valves. The number of valves is selected so that the converter can be operated with one or more failed

valves. This approach offers true redundancy as the converter can be operated at full power after failure.

One attractive realization of the bypass switch is a latching relay. A latching relay is often implemented similar to a conventional relay but with a permanent magnet in the magnetic path. A coil is energized which closes the relay. A permanent magnet holds the relay in its closed state even after the coil is de-energized. The bypass switch stays closed until it is manually reset.

The bypass switch needs power to operate, at least during closing. This power must be taken from the main circuit or supplied from ground potential.

The make time of an electro-mechanical bypass switch is several milliseconds and the valve must be protected by other means during this time. A Metal Oxide Varistor (MOV) may be sufficient to limit the voltage across the valve during closing of the switch. The varistor current may possibly be used to energize the bypass switch.

An electro-mechanical bypass switch will constitute a major part of the valve weight and volume. As the most voluminous component in the valve, it affects the layout of the valve.

3.4.6.2 Short Circuit Failure Mode

An alternative to the bypass switch is to use the Short Cirucit Failure Mode (SCFM) class of devices. These components are mechanically and electrically suited for series connection. Since they are guarantied to fail to short circuit fault protection is simplified. Some components are specified for continuous operation at full load current after failure. Examples of such components are ABB's StakPak [23] and Westcode Press-Pack IGBTs [24]. The high current rating of these components makes them suitable in converters for locomotives but not for EMUs.

3.4.6.3 Detection of Failed Components

If the degradation of the IGBT can be monitored actions can be taken in order to avoid a stopping failure. The degradation process is self enhancing in the sense that a degraded component will run hotter and the degradation process is accelerated. A component running hotter also risk failure due to operation outside the Safe Operating Area (SOA).

A way of detecting relative degradation of parallel IGBTs in a valve is described in [25]. The degradation of the parallel components is monitored by detecting an imbalance in the current sharing. If a component fails, the current will be unequally shared between components. The imbalance is detected and the valve is permanently short circuited by means of the remaining IGBTs. The remaining IGBTs are capable of conducting the full load current since they are no longer switched. Two different approaches for detecting the current imbalance are described. In the first method, the IGBTs are grouped into two groups and the current through the two groups are conducted in opposite direction through a sensing device, such as a Rogowski coil, measuring the resulting current difference. Another method, which may be more favourable in terms of valve integration for lower power levels, is to use shunt resistors as depicted in Figure 3.13.

Several actions can be taken when a failed or degraded component is detected. Gating the valve permanently on is most effective in hard switched applications where the ratio between switching losses and conduction losses are more equal. Another complication is the availability of power to supply the gate drive. Gating the valve permanently on, exclude the possibility to recover power from the snubbers or to draw power from the valve in the off state. Another option is to reduce the maximum power until the unit can be taken out of service and the valve can be replaced.

3.4.6.4 Multiple inverters

Two or more EMUs are normally operated permanently together as a train set. If each unit is equipped with its own line converter some redundancy

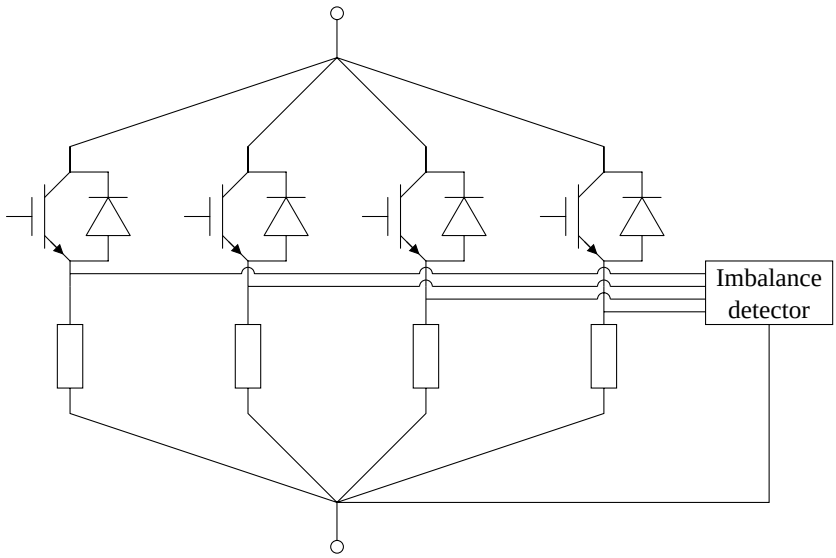

Figure 3.13: Current imbalance detector based on shunt resistors.

is provided. The train can continue to operate at reduced power until it can be taken out of service. Having one line converter per unit makes the EMU design more modular.

3.5 Filtering

The design of the line filter has not been considered in this thesis. Throughout the work, it has been assumed that the line filter can be implemented as a line reactor. The reactance has been assumed to be 20% which is slightly lower than the leakage reactance of a typical traction transformer.

In the proposed conversion system, the weight of the line filter becomes the dominating mass with a weight that surpasses the transformer weight. Therefore, reducing the weight of the line filter becomes a primary objective.

The dual bridge configuration and the high transformer frequency allow the front end converter control to be active up to the 1 kHz range. Thus, low

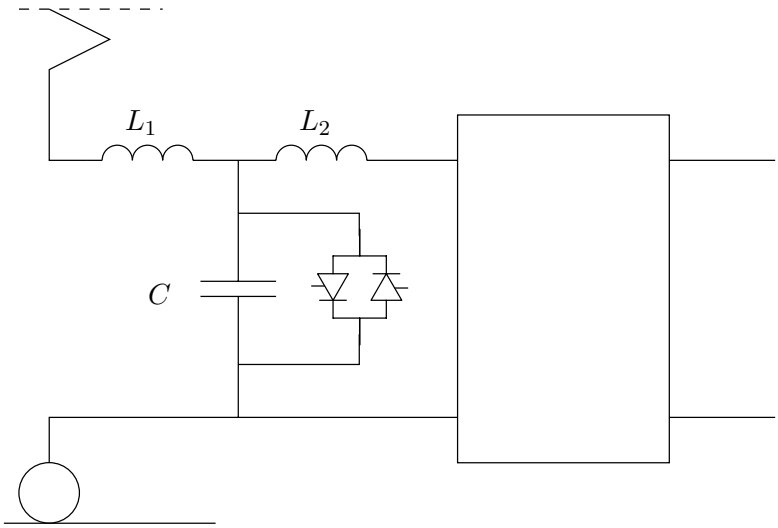

Figure 3.14: LCL line filter with thyristor crowbar.

order harmonics can be eliminated by control. Therefore, the size of line filter can be reduced considerably with respect to harmonic distortion.

The line filter plays an important role during fault. In case of failure, the primary converter can either be blocked or short circuited. If SCFM components are used, short circuiting the primary converter is safe. Any failed valves will go to short circuit in a safe fashion. However, if bonded components are used, the full line voltage will appear across a single subvalve which may lead to catastrophic failure. Instead, all valves are gated off and the energy stored in the line filer is dissipated in the primary converter. A MOV across each valve handles the energy stored in the filter.

The LCL filter approach (see Figure 3.14) reduce the amount of energy that has to be handled by the primary converter stage during fault and a thyristor crowbar can be used to protect the primary converter from the short circuit current. The crowbar cannot be placed directly across the primary converter due to the high voltage slope which would trigger the thyristor. Instead, the crowbar is placed across the filter capacitor.

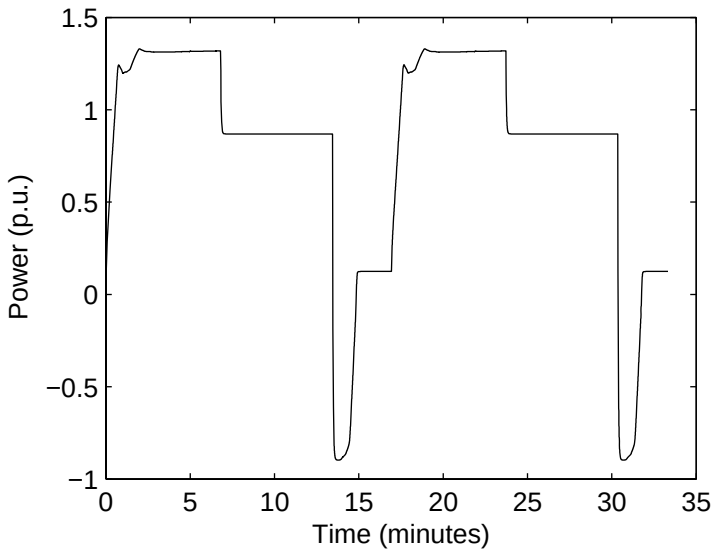

Figure 3.15: Drive cycle representing a typical regional train.

3.6 Drive Cycle Simulation

To give an indication of the efficiency of the system, simulations of key components have been carried out. The drive cycle used in the simulations, illustrated in Figure 3.15, represents a typical regional train. The top speed of the train is 200 km/h and the distance between stops is 40 km.

Losses in the VSC are calculated based on [Publication II] but scaled to represent a 1 MVA converter.

1700 V components are chosen for the reference implementation of the primary converter. The IGBTs are four parallel IXYS IXGH32N170A and the diodes are two parallel IXYS DH60-18A. The loss calcultation includes on state losses in the semiconductors as well as snubber losses. The device voltage is clamped to 1,5 times the DC-link voltage. On state voltage is taken from the device datasheet and the junction temperature is assumed to be 125 °C. Dynamic on state losses and ZCS losses are neglected.

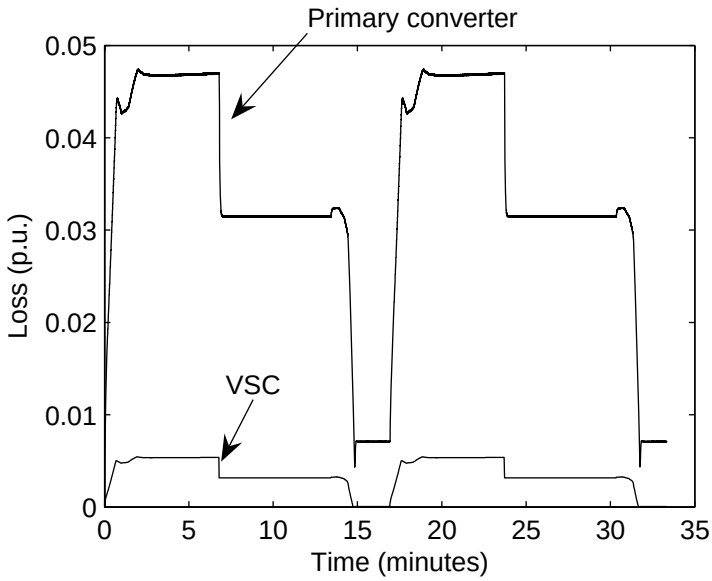

Figure 3.16: Semiconductor losses in the primary converter and VSC.

The semiconductor losses are shown in Figure 3.16. The total losses are dominated by the losses in the primary converter. The average loss in the primary converter is 3,5%. The transformer frequency is 4 kHz.

Table 3.3 shows the distribution of average losses during a drive cycle. The losses are normalized so that 100% corresponds to the total losses in an RC-snubbered primary converter with 1700 V IGBTs. Firstly, it is clear that there is a significant gain in replacing the RC-snubbers by a voltage clamping circuit. Second, minimum loss is achieved using 1200 V components. However, using 1200 V components are unpractical due to the total number of valves. Thus, 1700 V or 3300 V components are a good compromise.

No optimization of the converter configurations have been carried out. Thus, loss values should be considered indicative. There is a quick development on high voltage power devices and the optimum choice of technology and blocking voltage is a moving target. However, at the investigated frequency, 1700 V components with a clamping snubber result in a good compromise between switching losses and conduction losses. Its worth noting

Table 3.3: Loss distribution in the primary converter normalized to the losses of a converter with 1700 V components and RC-snubbers.

Subvalve blocking voltage	600 V	1200 V	1700 V	3300 V	
IGBT on-state losses	54	27	23	11	%
Diode on-state losses	42	21	18	7,7	%
RC-snubber losses	7,7	6,4	61	124	%
Voltage clamp	3,1	3,9	26	54	%
Total, RC-snubber	105	55	100	143	%
Total, voltage clamp	100	52	67	73	%

that for the active voltage clamp, described in [Publication IV], clamping losses are dissipated in the IGBT. Since the clamping losses are approximately equal to the on-state losses, power cycling is very low.

4 Prototype

An important objective of the project was to develop a close to full scale prototype. A description of the prototype system and some experimental results are given.

4.1 Main Circuit

In order to demonstrate the feasibility of the proposed converter system a prototype has been build. The prototype is a scaled version of a converter suitable for an EMU in Sweden.

Care has been taken so that the scaled system maintain approximately the same per-unit values as the full scale model where possible, which means that the prototype is not optimized for its rated power. Instead, each component was optimized for a full scale system and then scaled in order to maintain the same electrical and thermal behaviour. The voltage source converter was considered to be the most uncritical component of the system. Therefore, trade-offs were made on the VSC in order to maintain per-unit values for the transformer and cycloconverter.

The rated values of the modelled full scale converter are 1 MVA, 15 kV, and $16^2/_3$ Hz. The dual bridge configuration, illustrated in Figure 3.1, is assumed to be the most attractive topology. In the prototype only one of the two converter cells is implemented. The rated voltage was reduced to one third in order to simplify laboratory work.

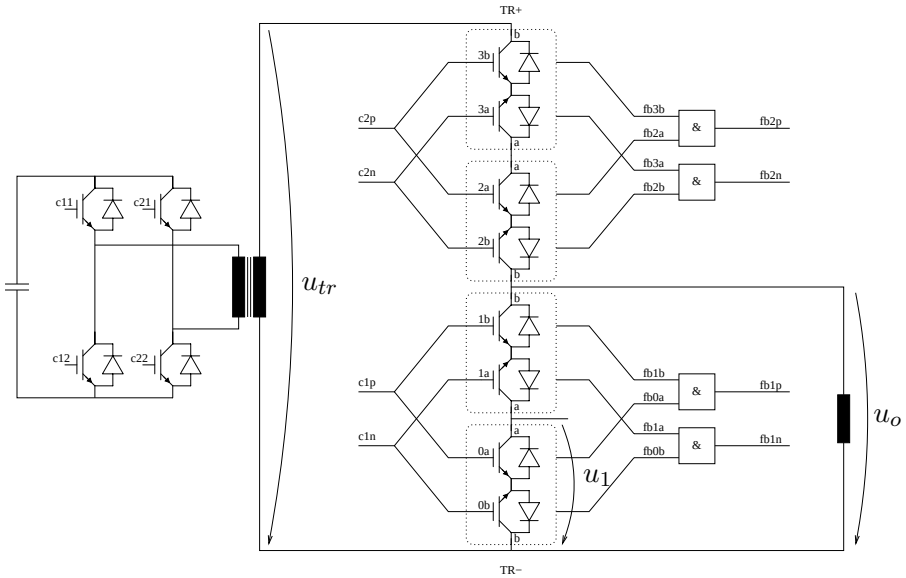

Figure 4.1: Main circuit of the prototype.

The prototype comprises a voltage source converter, a medium frequency transformer and a single cycloconverter leg loaded by an inductor. Figure 4.1 shows the main circuit and control and feedback signals.

4.2 Modulation and Control

The control and valve interface require a significant amount of dedicated logic. As much as possible of the logic was placed in configurable hardware to simplify the development process. Mainstream Field-Programmable Gate Arrays (FPGAs) can fit complex systems including Digital Signal Processor (DSP) functionality. Even the processor core may by synthesized and incorporated into the FPGA.

Two examples of commercially available cores are the Nios II from Altera [26], and the Microblaze from Xilinx [27]. Both processors are highly configurable and highly optimized for each manufacturer's FPGA design. However, these cores are closed source available under strict licenses.

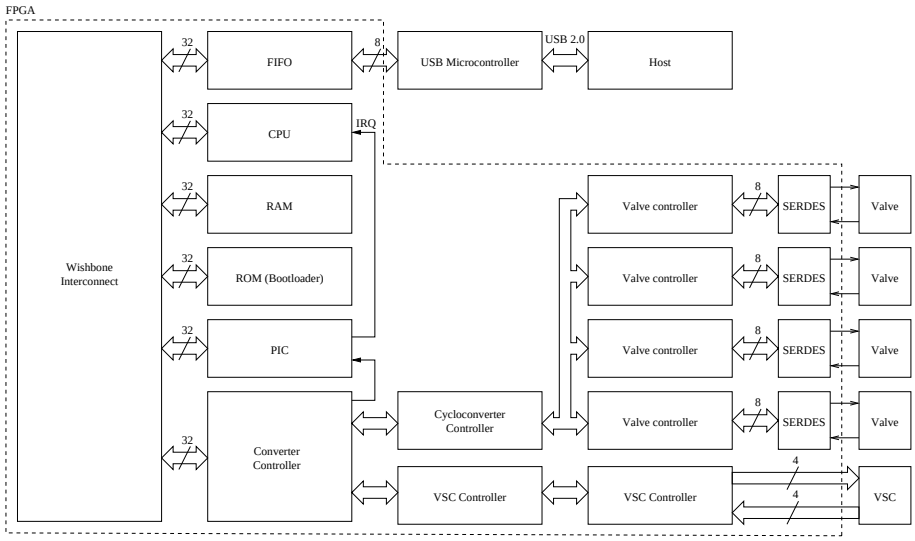

Figure 4.2: Functional overview of the control system.

There are also a number of target independent cores available under open source licenses. Examples of such cores, suitable for synthesis for FPGAs, are the AEMB [28] which is binary compatible to the Xilinx Microblaze, and the Micro32 [29] from Lattice. Both use the Wishbone bus which is an interconnection architecture suitable for System on Chip (SoC)-designs [30] . The Wishbone bus is in the public domain and a large number of Wishbone compliant open source Intellectual Property (IP) cores are available [31].

Figure 4.2 illustrate an overview of the control system. Most of the control functionality is implemented on the FPGA. The top level converter controller is implemented as a Wishbone compliant state machine controlling and monitoring the VSC controller and cycloconverter controller. The VSC controller and cycloconverter controller are implemented in a fashion similar to what is described in [32].

Figure 4.3 shows a simplified view of the state machine controlling the voltage source converter. The prototype converter consists of a single leg. Therefore, the prototype converter is not capable of soft-switching of the VSC. Therefore, capacitive snubbers have been left out and the VSC is

controlled in an open loop fashion. The transient states TR1 and TR2 correspond to dead time.

Figure 4.4 shows a simplified view of the state machine controlling the cycloconverter. As the purpose of the prototype was to demonstrate initialization and commutation of the primary converter only the commutation process corresponding to positive output current was implemented.

4.3 Cycloconverter

The cycloconverter consists of a string of series connected subvalves. The prototype subvalve is divided into a main circuit board containing main switches and drive circuitry (see Figure 4.5). A control board containing interface logic, control circuitry and power supplies is mounted on top of the main circuit board. The assembled subvalve is shown in Figure 4.6.

The main features of the prototype subvalve are:

- Active snubbing of the diode utilizing the IGBT as described in [Publication IV].
- Active control of the voltage slope during turn-on as described in [Publication IV].
- Snubber energy recovery for gate drive power supply as described in Section 3.4.3.
- Synchronization of the valve controller and subvalve as described in Section 3.4.4.
- Multiplexing of control signals over a single fibre as described in Section 3.4.4.

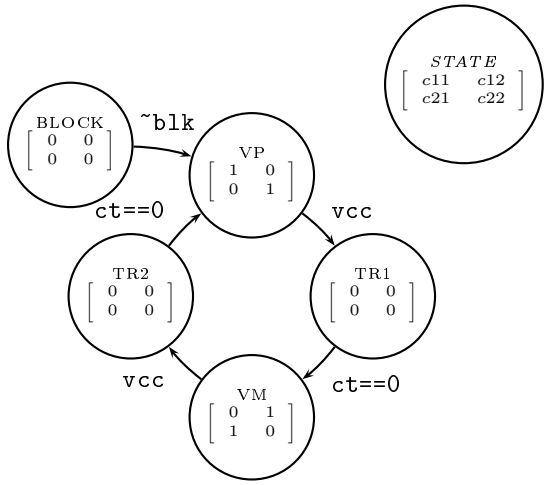

Figure 4.3: FSM for voltage source converter control.

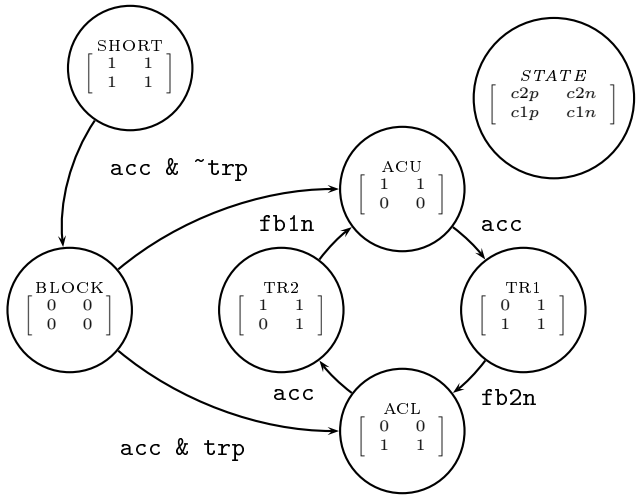

Figure 4.4: FSM for cycloconverter control.

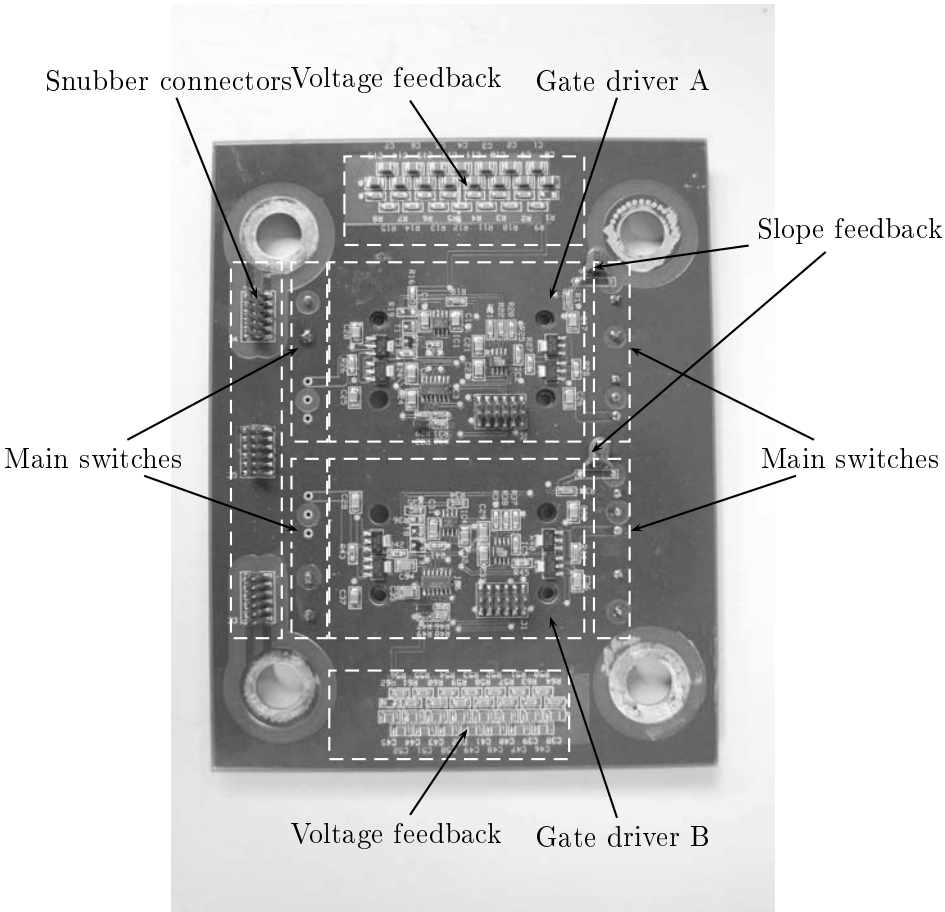

Figure 4.5: Driver and main circuit board.

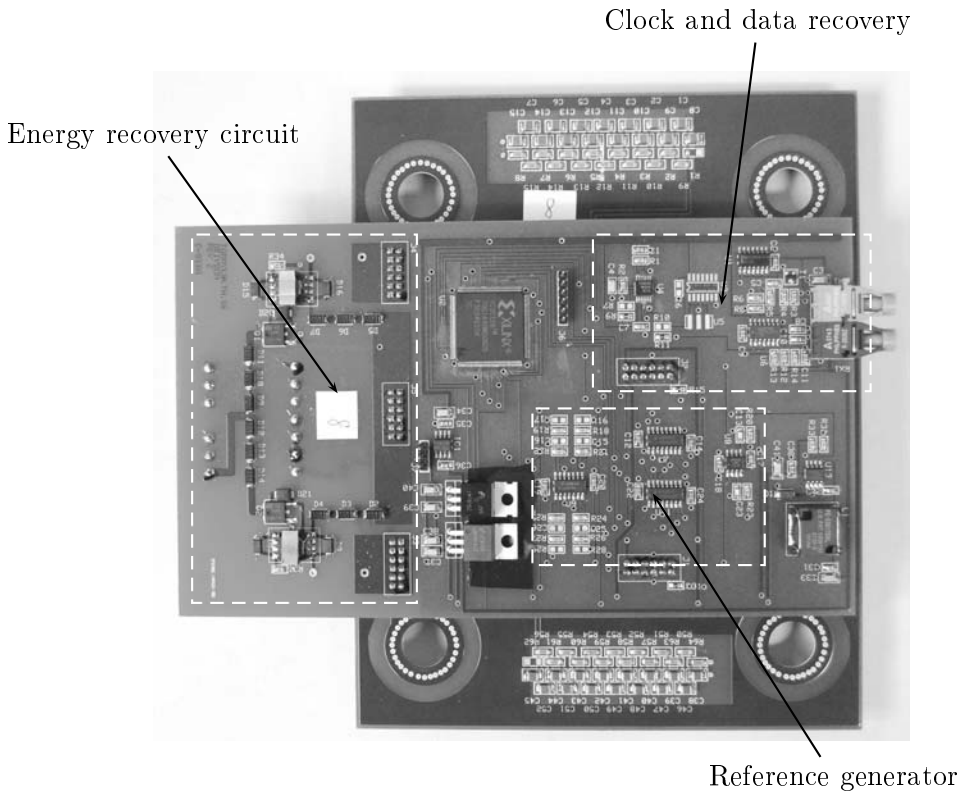

Figure 4.6: Assembled subvalve.

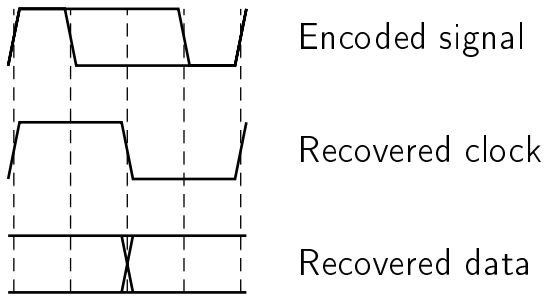

Figure 4.7: Clock and data encoding

4.3.1 Signalling

The same data link is used to distribute clock and data. In the prototype, the clock is encoded into the positive flank and data is encoded into the negative flank. The clock and data encoding scheme is illustrated in Figure 4.7. The advantage of this arrangement is that an extremely simple clock recovery circuit can be used. Infinite locking range of the Phase Locked Loop (PLL) eliminates the need for a precise clock reference in the valve. The required bandwidth is high compared to the signalling rate. However, that is of less importance due to the nature of the transmitted data.

The signalling circuit itself is capable of operating at a data rate of 50 MBaud. However, for simplicity the signalling circuit is operated at the system frequency which is 40 MHz, resulting in a data rate of 10 MBaud taking four times oversampling in the Serializer/Deserializer (SERDES) on the control system side into account. However, the valve is clocked at the same rate as the transmitted clock, i.e. 10 MHz. The word length is fixed at 8 databits plus start and stop bit resulting in a latency of approximately 1 µs.

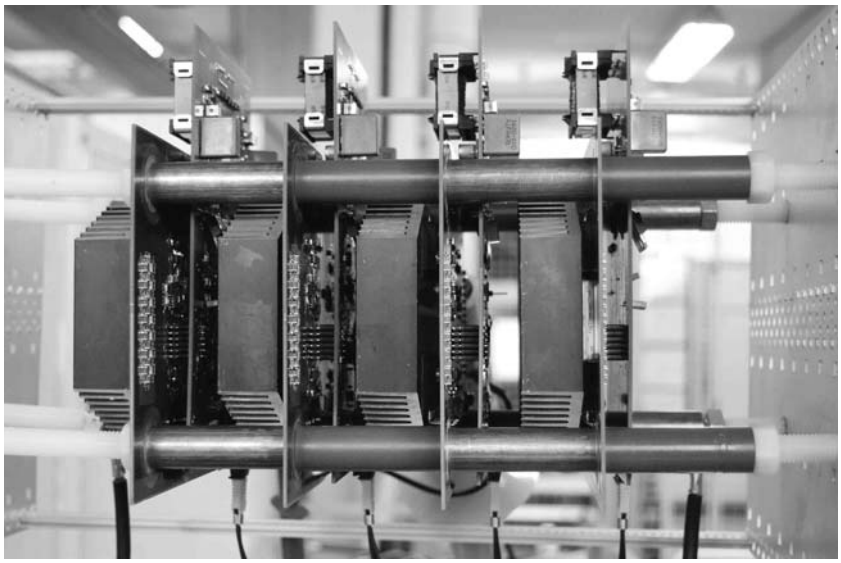

Figure 4.8: An assembled cycloconverter leg consisting of four series connected subvalves.

4.3.2 Cooling

The subvalves were designed for water cooling. However, the purpose of the initial testing of the cycloconverter was to demonstrate start-up and commutation of the valves and during evaluation the prototype was not run for more then a few seconds. Therefore, water cooling was abandoned and replaced by heatsinks cooled by natural convection. It should be possible to run the converter at rated load if the heatsinks are cooled by forced convection.

4.3.3 Interconnect

Figure 4.8 shows an assembled cycloconverter leg comprising two series connected subvalves per valve. The only connections to the subvalve are the main circuit terminals and a duplex fibre.

4.3.4 Power Supply

The power supply was implemented according to Section 3.4.3. No optimization of the power supply was carried out. In particular the transformer is considerably oversized. The transformer, which is visible in Figure 4.8, is the largest component in the valve.

4.3.5 Gate Drive and Snubber Circuit

The capacitive snubber is only active during diode recovery. The IGBT turn-on is performed without assistance of snubbers.

The prototype valves was equipped with fairly large turn-off snubbers ($C_s = 6{,}8\,\mathrm{nF}$) to allow easy start-up and operation at reduced voltage. By having large snubbers the converter can be started without increasing the transformer frequency during initialization.

4.3.6 Logic

The control logic was implemented in a ColdRunner Complex Programmable Logic Device (CPLD) from Xilinx. Due to the clock recovery circuit precise timing is achieved at low clock speed. Thus, energy consumption by the digital circuit is kept low. The voltage slope and clamp voltage references are programmed offline using Joint Test Action Group (JTAG). However, the hardware allows programming online via the optical interface if the appropriate software is implemented.

4.4 Transformer

The transformer was first optimized for full power and then scaled to maintain the same electrical and thermal properties. The height of the transformer winding was reduced to one third by removing turns from the pri-

Table 4.1: Selected prototype transformer data

Property	Symbol	Value
Base voltage	U_n	2,5 kV
Base power	S_n	168 kVA
Base current	I_n	67 A
Base frequency	f_n	$16^2/_3$ Hz
Rated transformer current	I_{tr}	53 A
Excitation voltage (sec)	U_d	600 V
Transformer frequency	f_{tr}	4 kHz
Primary turns	N_1	16
Secondary turns	N_2	2
Leakage inductance (primary)	L_k	35 µH
Efficiency	η	98%
Active weight	m	66 kg

mary winding; hence the same per-unit leakage inductance was maintained. Since the main heat flow is in the radial direction also the thermal properties are maintained. However, some properties do not scale very well. Since the secondary winding is a foil winding, the thickness of the secondary foil increase by a factor of three, thus increasing the eddy current losses significantly. Since the turn-ratio was maintained the excitation voltage had to be decreased from 1800 V to 600 V. The magnetizing inductance is determined by the air gap resulting from the cut. The core area is unaffected by the scaling but the number of secondary turns is decreased. Since the magnetizing inductance is proportional to the square of the number of turns, the magnetizing inductance decrease by a factor on nine. Thus, the reactive power consumption is significantly larger compared to the full scale transformer, even in absolute terms. A selected set of parameters for the prototype transformer is listed in Table 4.1.

The prototype transformer (see Figure 4.9) was immersed in oil.

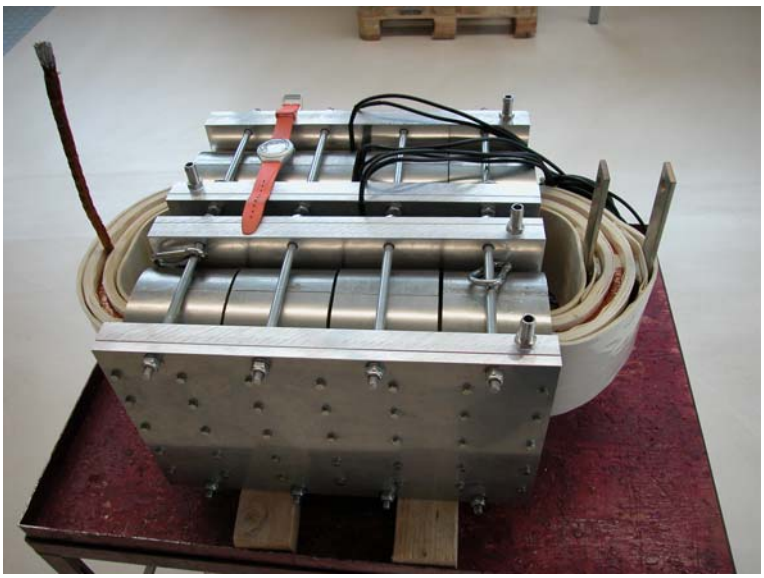

Figure 4.9: Prototype transformer before lowering into the tank

4.5 VSC

The VSC was operated at significantly lower voltage than what is typical in a full scale converter. The behaviour of the full scale inverter is investigated in [Publication II] and the VSC was considered to be the most uncritical component in the system. Therefore, compromises regarding scaling were made primarily to the VSC. The prototype VSC was operated without capacitive snubbers during the experiments since the prototype converter comprise only a single cycloconverter leg. Thus, the VSC can not be commutated under ZVS since there is no current to commutate the VSC when the load current freewheels through the cycloconverter.

4.6 Experimental Results

The purpose of the experimental investigation was to demonstrate initialization and successful commutation with series connected subvalves. The

converter is controlled in open loop and operated just for a few cycles. A single run of the prototype is divided into three stages:

Initialization A square wave voltage is applied to the cycloconverter. A fixed number of cycles, in the range of 5000 cycles, are applied. The local energy storage capacitors are charged and the valves are synchronized. The voltage level of the local energy storage is monitored and "Power OK" is signaled to the central controller. After the initialization procedure, the central controller proceeds to the run state if communication is established and all subvalves report successful initialization.

Run The converter is run for a predefined number of cycles. The commutation instance of the cycloconverter is programmed to a constant value.

Stop The run sequence is ended by blocking the VSC. After a short duration of time, all cycloconverter valves are short-circuited and the short-circuit is maintained until the valve is reset due to undervoltage.

Figure 4.10 shows the voltage across one valve and the corresponding snubber capacitors during the transition from initialization to run state. The converter has been operated at a constant frequency of 8 kHz and the snubbers are sized to allow start-up at reduced voltage. Therefore, the recovered power is 77 watts per valve during nominal operation. The power consumption of the valve is approximately 3 watts and the remaining power is dissipated in a zenerdiode protecting the voltage regulators. The valve is not able to operate under these conditions continuously. The waveforms in Figure 4.10 are in good agreement to the analytical results in Section 3.4.2. However, some additional energy transfer occurs due to the overvoltage during commutation. The prototype was operated with equal positive and negative pulse duration for clarity.

Figure 4.11 shows the voltage trajectories during commutation of the cycloconverter. The converter was operated at no load. The static voltage sharing error is approximately 5 % and the dynamic voltage sharing error is 10 %. The transformer voltage is effectively clamped. Compared to mea-

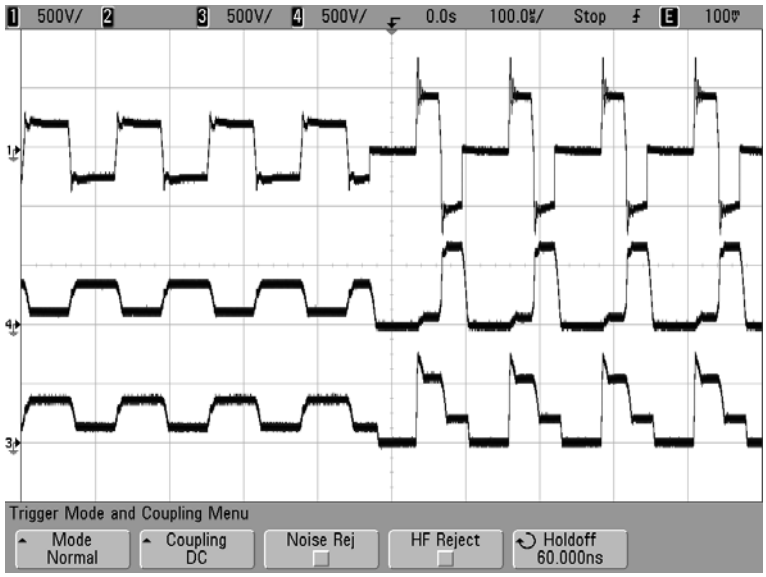

Figure 4.10: Valve initialization: Valve voltage (1) and snubber capacitor voltages (3&4).

surements in [Publication IV] the gate driver is operated without snubbers during turn-on. As a result, a small overshoot during turn-on is visible.

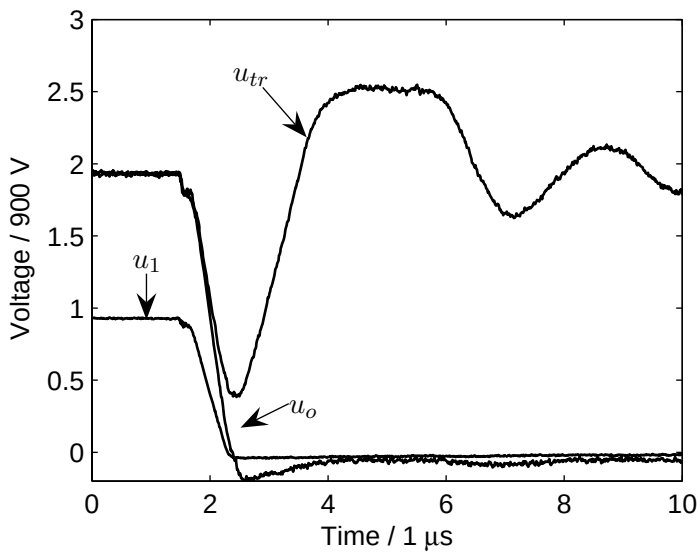

Figure 4.11: Voltage trajectories during commutation at no-load.

5 Conclusions and Future Work

This chapter summarizes the conclusions of the work. Some directions for future development, mainly regarding the laboratory prototype, are given.

5.1 Conclusions

A suitable transformer frequency has been deduced based on the capabilities of the primary converter [Publication II]. The switching losses under ZVS were derived by means of single pulse measurements on 3,3 kV NPT IGBTs. The maximum switching frequency for a converter based on the MCC topology could be increased beyond 4 kHz compared to approximately 500 Hz in a conventional traction inverter without decreased efficiency.

The influence of the low order harmonics associated with the constrained modulation of the MCC has been investigated. It was found that the dual-bridge configuration provide an effective way of minimizing the low order harmonics [Publication III]. The psophometric current, which is a measure of the currents influence on telecommunication, can be reduced to a level one decade below the limit for a four kilohertz system by proper modulation.

A transformer topology suitable for EMU applications has been presented. The topology is characterized by a simple winding arrangement without direct cooling of the high voltage winding [Publication I]. Thus, it is mainly attractive in the lower power range. For transformers in the higher power range, like locomotives, other types of transformers will probably be more suitable. The proposed topology is equally suited for dry insulation as oil immersed insulation. An oil immersed design was chosen due to its good dielectric performance. The specific weight of the transformer was found

to be 0,23 kg/kVA for a four kilo-hertz transformer with an amorphous core. This is more than twice the weight reported for competing topologies. However, the studied transformer has a high turn ratio and is based on an inexpensive core material mass produced for distribution transformers while the competing design was a dry insulated coaxial transformer with a unity turn-ratio and nanocrystalline core. The competing design was also designed for a higher power range.

A cycloconverter subvalve suitable for series connection has been build and tested [Publication IV]. The active gate control offers tight control of the voltage slope during transition independent of the device characteristics. The proposed control method allows reduction of the commutation speed without increasing the commutation delay. Reducing the commutation speed has a positive impact on the intrawinding voltage distribution. Since the valve turns on against the inductance of the transformer, the influence on the switching losses is minimal. Further, the IGBT is used in it linear region in order to clamp the voltage across the anti-parallel diode during reverse recovery. Thus, the need for a big external snubber is eliminated. Only a small external snubber is used to limit the initial voltage slope during reverse recovery and to provide power for the gate drive. A circuit to recover the snubber energy to power the valve has been presented.

A prototype of the studied converter system has been build. The prototype consists of a single converter cell only and the voltage was reduced to one third in order to simplify laboratory work. The prototype was first optimized for a power level suitable for an EMU (1 MVA) and then scaled. The purpose of doing so was to resemble the electrical and thermal properties of the full scale system as closely as possible. Thus, the laboratory prototype is suboptimal with respect to weight. Most of the electrical and thermal properties scale very well. However, an important exception is the magnetizing current which is significantly larger in the scaled prototype compared to the full scale transformer.

The efficiency of the proposed converter structure has been determined by drive cycle simulations corresponding to a regional train. The conversion losses was found to be similar to a conventional traction transformer and hard switched LCM. The losses originate mainly from diode reverse re-

covery losses and conduction losses in the primary converter stage. The loss estimation is based on first generation NPT IGBTs and there has been a rapid development on high voltage IGBTs since. An improved diode with lower reverse recovery current would decrease snubber losses and allow increased blocking voltage leading to less on-state losses. Commercially available Silicon Carbide (SiC) schottky diodes have reached 1200 V and SiC bipolar diodes are under development. The bipolar SiC diode, featuring almost no reverse recovery, would be the perfect device for the source commutated converter.

Some initial testing of the prototype has been performed. The aim of the prototype test was to demonstrate initialization and commutation of the cycloconverter with series connected valves. No effort has been made to implement the MCC modulation pattern. The feasibility of the MCC modulation pattern has been investigated previously by others. The efficiency improvements on the VSC side due to ZVS was assumed to be proved by the single pulse measurements.

The main advantage of the studied topology is the simple layout of the primary converter. Others report no or only marginal reduction of the volume of the MF system. This is assumed to be mainly due to the high number of separately insulated modules and high component count on the high voltage side. The proposed converter concept allows high integration of the primary converter.

5.2 Future Work

At the time of writing this thesis only limited testing of the prototype converter has been performed.

The number of subvalves in the cycloconverter leg should be extended. During the initial testing only two series connected valves were used. The monitoring function must be extended to avoid damage to the subvalves in case of failure.

The converter should be operated continuously. Several changes would have to be made to the prototype in order to operate it continuously. During initial testing an over-sized snubber was used in order to allow initialization of the cycloconverter valves without increase of the switching frequency and operation at supply voltage below the rated value. The valve will not be able to dissipate the power continuously with the present snubbers. Therefore, the size of the snubber should be decreased and the modulation logic and control software must be changed to allow change of modulation frequency online.

Implementing the MCC modulation requires the addition of a second cycloconverter leg. Further, the resonant commutation during low load has to be investigated in combination with series connection of subvalves on the primary side.

The converter valves will not operate continuously at rated load when cooled by natural convection. Possibly, forced convection by means of a fan will be enough. Loading the converter at rated load constitutes a problem in it self.

Justification of the MF topology is not complete without experimental verification of the efficiency. However, the VSC operate at only 600 V DC-link voltage which is not representative for a traction drive. At least the efficiency of the MF transformer and primary converter should be studied further.

The line filter should be further examined since it is the heaviest component of the proposed MFT concept. Further, the line filter plays in important role concerning protection of the primary converter.

In this thesis, it is suggested that the subvalve can be highly integrated. By integrating the driver and main circuit, using only Surface Mounted Devices (SMDs), the size of the subvalve and, thus, the primary converter can be very small. However, the reliability of such a valve should be investigated.

References

[1] H. Menniken, "Stromrichtersystem mit wechsel-spannungs-zwischenkreis und seine anwendung in der traktionstechnik," Ph.D. dissertation, Fakultät für Elektrotechnik, RWTH Aachen, Aachen, Germany, 1978.

[2] S. Östlund, "A primary switched converter system for traction applications," Ph.D. dissertation, Royal Institute of Technology, Stockholm, Sweden, December 1992.

[3] M. Steiner, R. Deplazes, and H. Stemmler, "A new transformerless topology for AC-fed traction vehicles using multi-star induction motors," in *8th European Conference on Power Electronics and Applications*, Lausanne, Switzerland, 1999.

[4] P. Kjaer, S. Norrga, and S. Östlund, "A primary-switched line-side converter using zero voltage switching," in *Conference Record of the IEEE Industry Applications Conference*, vol. 4, 8-12 Oct. 2000, pp. 2361–2368.

[5] M. Steiner, "Seriegeschaltete gleichenspannungszwischenkreisumrichter in traktionsanwendungen am wechselspannungsfahrdraht," Ph.D. dissertation, ETH, 2000.

[6] S. Norrga, "A soft-switched bi-directional isolated AC/DC converter for AC-fed railway propulsion applications," in *Procedings of the IEE International conference on Power Electronics and Electrical Machines (PEMD)*, Bath, United Kingdom, apr 2002.

[7] B. Engel, M. Victor, G. Bachmann, and A. Falk, "15 kV/16.7 Hz energy supply system with medium frequency transformer and 6.5 kV IGBTs in resonant operation," in *Eurpean Conference on Power Electronics and Applications, Toulouse, France*, 2003.

[8] M. Glinka and R. Marquardt, "A new AC/AC-multilevel converter family applied to a single-phase converter," in *The Fifth International Conference on Power Electronics and Drive Systems, PEDS*, vol. 1, 17-20 Nov. 2003, pp. 16–23.

[9] A. Rufer, N. Schibli, C. Chabert, and C. Zimmermann, "Configurable front-end converters for multicurrent locomotives operated on 16 2/3 Hz AC and 3 kV DC systems," *IEEE Transactions on Power Electronics*, vol. 18, pp. 1186–1193, Sep. 2003.

[10] N. Hugo, P. Stefanutti, M. Pellerin, and A. Akdag, "Power electronics traction transformer," in *European Conference on Power Electronics and Applications*, 2-5 Sept. 2007, pp. 1–10.

[11] M. Steiner and H. Reinhold, "Medium frequency topology in railway applications," in *European Conference on Power Electronics and Applications*, Aalborg, 2007.

[12] Banverket, "Fordon - elektriska krav. Krav för kompatibilitet med den elektriska infrastrukturen och andra fordon," Swedish Railway Administration, 2007.

[13] G. Asplund, K. Eriksson, and K. Svensson, "DC transmission based on voltage source converters," in *CIGRE SC14 Colloquium*, South Africa, 1997.

[14] A.-C. Rufer, N. Schibli, and C. Briguet, "A direct coupled 4-quadrant multilevel converter for 16 2/3 Hz traction systems," in *Sixth International Conference on Power Electronics and Variable Speed Drives (Conf. Publ. No. 429)*, 23-25 Sept. 1996, pp. 448–453.

[15] H. Reinold and M. Steiner, "Characterization of semiconductor losses in series resonant DC-DC converters for high power appications using

transformers with low leakage inductance," in *8th European Conference on Power Electronics and Applications*, Lausanne, Switzerland, 1999.

[16] L. Heinemann, "An actively cooled high power, high frequency transformer with high insulation capability," in *Seventeenth Annual IEEE Applied Power Electronics Conference and Exposition, APEC*, vol. 1, 10-14 March 2002, pp. 352–357.

[17] K. Sadahiro, S. Gotoh, and S. Uenosono, "Soft magnetic materials of JFE steel group," JFE Steel, Tech. Rep. 6, oct 2005.

[18] G. Herzer, "Amorphous and nanocrystaline soft magnetics," in *Proceedings of the NATA Advanced Study Insitute on Magnetic Hysteresis in Novel Materials*, 1996.

[19] S. Larsson, "On the design of a bi-directional power valve for natural commutation," Master's thesis, KTH Electrical Engineering, Stockholm, Sweden, 2004.

[20] S. Norrga, "On soft-switching isolated AC/DC converters without auxiliary circuits," Ph.D. dissertation, KTH, Stockholm, Sweden, 2005.

[21] W. McMurray, "Optimum snubbers for power semiconductors," *IEEE Trans. Ind. Appl. (USA)*, vol. 1A-8, no. 5, pp. 593 – 600, 1972.

[22] J. Holtz and R. Rosner, "Gate drive power recovery and regenerative snubber scheme for series-connected GTOs in high voltage inverters," in *Conference Record of the IEEE Industry Applications Conference, Thirty-Fourth IAS Annual Meeting.*, vol. 3, 3-7 Oct. 1999, pp. 1535–1540.

[23] *StakPak IGBT Press-packs: A new Packaging Concept for High Power Electronics*, ABB. [Online]. Available: http://www.abb.com

[24] *Press-Pack IGBTs*, Westcode, May 2006. [Online]. Available: http://www.westcode.com

[25] H. P. Nee, "Converter valve," Patent WO 2006/104430 A1, October 2006.

[26] *Nios II Processor Reference Handbook*, 9th ed., Altera Corporation, mar 2009.

[27] *MicroBlaze Processor Reference Guide*, v9.0 ed., Xilinx.

[28] *AEMB 32-bit Microprocessor Core*, Aeste Works. [Online]. Available: http://www.aeste.net/

[29] *LatticeMico32 Processor Reference Manual*, Lattice Semiconductor Corporation, November 2008.

[30] *WISHBONE System-on-Chip (SoC) Interconnection Architecture for Portable IP Cores*, B.3 ed., OpenCores.org, September 2002. [Online]. Available: http://opencores.org/

[31] "OpenCores website." [Online]. Available: http://www.opencores.org

[32] S. Norrga, S. Meier, and S. Östlund, "A three-phase soft-switched isolated AC/DC converter without auxiliary circuit," in *Conference Record of the 2004 IEEE Industry Applications Conference, 39th IAS Annual Meeting*, vol. 3, 3-7 Oct. 2004, pp. 1768–1775.

List of Acronyms

AC	Alternating Current
ACM	Auxiliary Converter Module
CPLD	Complex Programmable Logic Device
DC	Direct Current
DSP	Digital Signal Processor
EMI	Electro Magnetic Interference
EMU	Electric Multiple Unit
FIT	Failure in Time
FPGA	Field-Programmable Gate Array
GTO	Gate Turn-off Thyristor
HVDC	High Voltage Direct Current
IGBT	Insulated Gate Bipolar Transistor
IP	Intellectual Property
JTAG	Joint Test Action Group
LCM	Line Converter Module
M^2LC	Modular Multilevel Converter

MCC	Mutually Commutated Converter
MCM	Motor Converter Module
MF	Medium Frequency
MFT	Medium Frequency Transformer
MOV	Metal Oxide Varistor
NPC	Neutral Point Clamped
NPT	Non-Punch Through
PLL	Phase Locked Loop
PT	Punch Through
SCFM	Short Cirucit Failure Mode
SERDES	Serializer/Deserializer
SiC	Silicon Carbide
SMD	Surface Mounted Device
SOA	Safe Operating Area
SoC	System on Chip
SPT	Soft Punch Through
VSC	Voltage Source Converter
ZCS	Zero Current Switching
ZVS	Zero Voltage Switching